Available online at www.sciencedirect.com

ScienceDirect

Geochimica et Cosmochimica Acta 134 (2014) 74–99

Geochimica et Cosmochimica Acta

www.elsevier.com/locate/gca

Carbon isotope and abundance systematics of Icelandic geothermal gases, fluids and subglacial basalts with implications for mantle plume-related CO_2 fluxes

P.H. Barry [a,b,*], D.R. Hilton [a], E. Füri [a,c], S.A. Halldórsson [a], K. Grönvold [d]

[a] *Fluids and Volatiles Laboratory, Scripps Institution of Oceanography, UCSD, La Jolla, CA 92093-0244, USA*

[b] *Now at Planetary Geosciences Institute, Department of Earth Planetary Sciences, University of Tennessee, Knoxville, TN 37996-1410, USA*

[c] *Now at Centre de Recherches Pétrographiques et Géochimiques, CNRS-UL, 15 rue Notre-Dame des Pauvres, BP20, 54501 Vandoeuvre-lès-Nancy Cedex, France*

[d] *Nordic Volcanological Centre, Institute of Earth Sciences, University of Iceland, Askja, Sturlugata 7, IS-101 Reykjavik, Iceland*

Received 19 July 2013; accepted in revised form 26 February 2014; available online 13 March 2014

Abstract

We report new carbon dioxide (CO_2) abundance and isotope data for 71 geothermal gases and fluids from both high-temperature (HT > 150 °C at 1 km depth) and low-temperature (LT < 150 °C at 1 km depth) geothermal systems located within neovolcanic zones and older segments of the Icelandic crust, respectively. These data are supplemented by CO_2 data obtained by stepped heating of 47 subglacial basaltic glasses collected from the neovolcanic zones. The sample suite has been characterized previously for He–Ne (geothermal) and He–Ne–Ar (basalt) systematics (Füri et al., 2010), allowing elemental ratios to be calculated for individual samples. Geothermal fluids are characterized by a wide range in carbon isotope ratios ($\delta^{13}C$), from −18.8‰ to +4.6‰ (vs. VPDB), and $CO_2/^3He$ values that span eight orders of magnitude, from 1×10^4 to 2×10^{12}. Extreme geothermal values suggest that original source compositions have been extensively modified by hydrothermal processes such as degassing and/or calcite precipitation. Basaltic glasses are also characterized by a wide range in $\delta^{13}C$ values, from −27.2‰ to −3.6‰, whereas $CO_2/^3He$ values span a narrower range, from 1×10^8 to 1×10^{12}. The combination of both low $\delta^{13}C$ values and low CO_2 contents in basalts indicates that magmas are extensively and variably degassed. Using an equilibrium degassing model, we estimate that pre-eruptive basaltic melts beneath Iceland contain ~531 ± 64 ppm CO_2 with $\delta^{13}C$ values of −2.5 ± 1.1‰, in good agreement with estimates from olivine-hosted melt inclusions (Metrich et al., 1991) and depleted MORB mantle (DMM) CO_2 source estimates (Marty, 2012). In addition, pre-eruptive CO_2 compositions are estimated for individual segments of the Icelandic axial rift zones, and show a marked decrease from north to south (Northern Rift Zone = 550 ± 66 ppm; Eastern Rift Zone = 371 ± 45 ppm; Western Rift Zone = 206 ± 24 ppm). Notably, these results are model dependent, and selection of a lower $\delta^{13}C$ fractionation factor will result in lower source estimates and larger uncertainties associated with the initial $\delta^{13}C$ estimate. Degassing can adequately explain low CO_2 contents in basalts; however, degassing alone is unlikely to generate the entire spectrum of observed $\delta^{13}C$ variations, and we suggest that melt–crust interaction, involving a low $\delta^{13}C$ component, may also contribute to observed signatures. Using representative samples, the CO_2 flux from Iceland is estimated using three independent methods: (1) combining measured $CO_2/^3He$ values (in gases and basalts) with ^3He flux estimates (Hilton et al., 1990), (2) merging basaltic emplacement rates of Iceland with pre-

* Corresponding author at: Planetary Geosciences Institute, Department of Earth Planetary Sciences, University of Tennessee, Knoxville, 37996-1410, USA. Tel.: +1 3157295696.

E-mail address: peter.barry@utk.edu (P.H. Barry).

http://dx.doi.org/10.1016/j.gca.2014.02.038

eruptive magma source estimates of ~531 ± 64 ppm CO_2, and (3) combining fluid CO_2 contents with estimated regional fluid discharge rates. These methods yield CO_2 flux estimates from of 0.2–23 × 10^{10} mol a^{-1}, which represent ~0.1–10% of the estimated global ridge flux (2.2 × 10^{12} mol a^{-1}; Marty and Tolstikhin, 1998).

1. INTRODUCTION

The study of carbon dioxide (CO_2) emitted in magmatically-active regions provides insight into fluxes associated with volatile transfer from Earth's interior to the surface, the interaction history of magmatic and crustal reservoirs, and the nature of those reservoirs and how they contribute to the deep carbon cycle (Marty and Jambon, 1987; Varekamp et al., 1992; Marty and Tolstikhin, 1998; Dasgupta and Hirschmann, 2010). In this respect, Iceland is of particular interest due to its unique geological setting, marking the intersection of plume-related magmatism (as traced by the ubiquitous presence of high $^3He/^4He$ ratios throughout Iceland, e.g., Füri et al., 2010 and references therein) with the mid-Atlantic Ridge. Moreover, potential sampling opportunities are abundant throughout the Icelandic crust (rifting, non-rifting, and older regions) due to easy access in a subaerial environment to both contemporary geothermal degassing and extensive Neogene volcanism.

The importance of CO_2 lies in the fact that it comprises the major non-aqueous constituent of magmatic gases and serves as the principal carrier gas for other trace volatile species, such as the noble gases. In basaltic magmas, a CO_2-rich gas phase is typically present due to the relative insolubility of CO_2 and consequent transfer from melt to vapor during magma ascent (e.g., Dixon and Stolper, 1995). Thus, by investigating the CO_2 characteristics of glassy rims of rapidly quenched pillow lavas, a number of intrinsic melt properties, including source volatile concentrations, storage depths, and transport rates through the crust may be examined (Macpherson and Mattey, 1994; Macpherson et al., 2005a). A complementary approach is to target the CO_2 characteristics of geothermal systems of Iceland (Arnórsson and Barnes, 1983; Sano et al., 1985; Poreda et al., 1992; Hilton et al., 1998b). Using knowledge of aqueous fluid and/or heat fluxes from the Icelandic crust, estimates of associated CO_2 fluxes from the melt source region are possible. This is important because estimates of plume-related CO_2 fluxes (~3 × 10^{12} mol a^{-1}; Marty and Tolstikhin, 1998) are on par with CO_2 releases from mid-ocean ridges. To date, however, there are relatively few detailed studies focusing on the CO_2 systematics in plume-related magmatic regions.

Here, we present new carbon (isotope and abundance) data for both subglacial glasses of the neovolcanic zones as well as high- and low-temperature geothermal fluids from on- and off-axial regions of Iceland, respectively. These new data are combined with previously published noble gas (He–Ne–Ar) measurements on the same sample suite (Füri et al., 2010) to discern the underlying processes controlling CO_2 abundance, isotope variations, and CO_2–noble gas relationships. By investigating degassing models for subglacially-emplaced basalts, we estimate the carbon concentration and isotope characteristics of pre-eruptive melts, representing various segments of the underlying Icelandic mantle. In addition, we identify other processes that may act to modify initial CO_2 compositions and thus contribute to a skewed or biased representation of the CO_2 distribution throughout Iceland. Our aim is to better characterize CO_2 abundances, elemental ratios (e.g., $CO_2/^3He$), and $\delta^{13}C$ values of the Icelandic mantle source, thus providing a clearer picture of the carbon characteristics of mantle plume sources. Using these new data, we are able to formulate three independent estimates of the CO_2 flux associated with degassing of the Icelandic mantle and thus gain further insight into how the deep carbon cycle interacts with surficial reservoirs.

2. GEOLOGICAL SETTING AND PRIOR STUDIES

Iceland is a ~100,000 km^2 subaerial segment of the Mid-Atlantic Ridge, marked by enhanced crustal thickness resulting from anomalous melting associated with a mantle hotspot (White et al., 1995; Bjarnason et al., 1996; Darbyshire et al., 2000; Bjarnason and Schmeling, 2009). Three-dimensional seismic tomography studies show the existence of a cylindrical-to-tabular shaped zone of low P- and S-wave velocities beneath central Iceland, suggesting that the underlying mantle consists of a hot, narrow conduit of upwelling asthenosphere (Wolfe et al., 1997). However, the depth of the conduit is widely debated, with somemodels indicating that the low velocity anomaly is confined to the upper mantle (Ritsema et al., 1999; Foulger et al., 2000, 2001), while others suggest that the seismic velocity anomaly may extend as deep as the core-mantle boundary (Helmberger et al., 1998; Bijwaard and Spakman, 1999; Zhao, 2004), which is consistent with the mantle plume hypothesis (Morgan, 1971).

Recent volcanic activity on Iceland is widespread and occurs in two types of neovolcanic zones – axial rift zones and off-rift volcanic flank zones – with individual volcanic systems typically comprised of a central volcano and/or surrounding fissure swarms (Sæmundsson, 1978; Jakobsson and Gudmundsson, 2008). Axial rift zones traverse Iceland, connecting the adjacently located submarine Reykjanes and Kolbeinsey ridges: thus, they represent the on-land equivalent of mid-ocean-ridge type spreading. In southern Iceland, the axial rift zone is subdivided into the Western (WRZ) and Eastern (ERZ) Rift Zone segments, which are separated by a transform fault system known as the South Iceland Seismic Zone (SISZ) (Fig. 1). The axial rift zone system, which erupts lavas of tholeiitic composition, extends to the north of the Vatnajökull glacier and towards the Kolbeinsey Ridge along the Northern Rift Zone (NRZ).

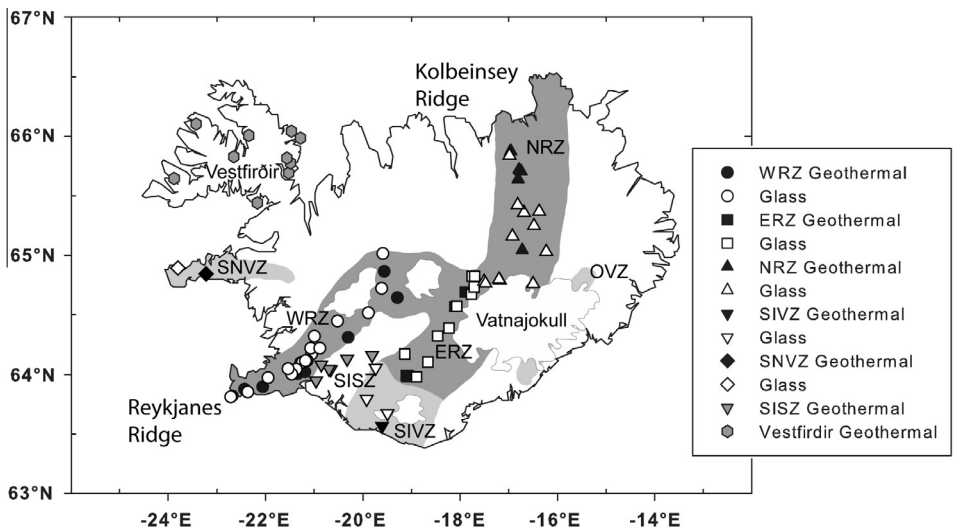

Fig. 1. Map of Iceland showing neovolcanic rift zones, sample locations, and the location of current glacial cover. The Western (WRZ), Eastern (ERZ), and Northern rift zones (NRZ) are shaded with dark grey, whereas transitional-alkalic to alkalic off-axis volcanic zones, i.e., the South Iceland Volcanic Zone (SIVZ), Snæfellsnes Volcanic Zone (SNVZ), and Öræfajökull Volcanic Zone (OVZ), are shown in light grey. Also shown are the South Iceland Seismic Zone (SISZ), Vestfirðir (the northwest peninsula of Iceland), and the adjacent submarine Reykjanes and Kolbeinsey ridge segments. Sample locations for geothermal fluids are denoted with closed symbols and open symbols are used for basalts.

The off-axis volcanic flank zones consist of the South Iceland Volcanic Zone (SIVZ), the Snæfellsnes Volcanic Zone (SNVZ), and the Öræfajökull Volcanic Zone (OVZ) – all located on older basement and distinguished by slightly more alkalic volcanism (Oskarsson et al., 1982; Jakobsson et al., 2008). Finally, the off-axis Vestfirðir region in northwest Iceland is characterized by tholeiitic lavas that range in age from ~16 to 9 Myr (McDougall et al., 1984; Hardarson et al., 1997).

The geochemical evolution of Iceland likely involves mixing of a variety of mantle endmember compositions – both enriched, and presumably plume-related and depleted, akin to DMM – pointing to significant heterogeneity in mantle sources feeding the neovolcanic zones (Schilling, 1973; Hart et al., 1973; Sun et al., 1975; Thirlwall et al., 2004; Peate et al., 2010). In terms of helium, high $^3He/^4He$ ratios (up to ~34 R_A) are found in central Iceland in the ERZ and the SIVZ (Condomines et al., 1983; Kurz et al., 1985; Hilton et al., 1990; Breddam et al., 2000; Macpherson et al., 2005b; Füri et al., 2010), consistent with seismic investigations, which place the hypothesized center of the Icelandic hotspot under central Iceland (Tryggvason et al., 1983; Wolfe et al., 1997). However, even higher $^3He/^4He$ values are found off-axis, in Tertiary basalts of Vestfirðir (Hilton et al., 1999; Ellam and Stuart, 2004). In addition to mantle source variations, there is evidence for crustal modification, and several oxygen isotope studies of Icelandic basalts suggest involvement of near surface crustal assimilation (e.g., Muhlenbachs et al., 1974; Burnard and Harrison, 2005) and/or recycled oceanic crust in the enriched mantle source (e.g., Macpherson et al., 2005b; Thirlwall et al., 2006).

Basaltic CO_2 abundance and isotope studies of Icelandic subglacial basalts are relatively few, due to the highly degassed nature and typically low CO_2 abundances (i.e.,<30 ppm; Höskuldsson et al., 2006; Tuffen et al., 2010). However, studies of HT geothermal systems in the axial rift zones indicate that the Icelandic-plume mantle source is characterized by $\delta^{13}C$ values $\sim -3.8 \pm 0.7‰$ (Poreda et al., 1992), significantly higher than the observed range of $-16‰$ to $-6‰$ in off-axis regions (e.g., Vestfirðir; Hilton et al., 1998b). In this respect, axial rift zone $\delta^{13}C$ values overlap with the high-end of DMM-like $\delta^{13}C$ values ($-5 \pm 1‰$; Marty and Zimmermann, 1999; Cartigny, 2005). At this point, however, it is worth pointing out that there is considerable uncertainty regarding the $\delta^{13}C$ value (and range) of DMM, with various groups using different estimates. For example, $\delta^{13}C$ values of $-6 \pm 1‰$ (Des Marais and Moore, 1984), $-5.9 \pm 1.6‰$ (Mattey et al., 1984), $-5.5 \pm 0.5‰$, (Deines et al., 1987), $-4‰$ (Javoy and Pineau, 1991), $-5.2 \pm 0.7‰$ (Marty and Zimmermann, 1999), $-6.5 \pm 2‰$ (Sano and Marty, 1995), $-5 \pm 1‰$ (Cartigny et al., 1997, 1998 and Cartigny, 2005), $-4.5‰$ (Fischer et al., 2009), and $-4 \pm 3‰$ (Palot et al., 2012) have all been adopted for DMM. Based on the large dataset ($n = 4400$) compiled for diamonds by Cartigny (2005), and the overall agreement with Marty and Zimmermann (1999), who compiled a global (basalt) dataset, we adopt a DMM $\delta^{13}C$ value of $-5 \pm 1‰$ vs. Vienna Pee Dee Belemnite (VPDB) in further discussions.

The ratio of CO_2 to ^3He ($CO_2/^3He$) of HT geothermal systems range from 0.6 to 14×10^9, with an average value of $\sim 6 \times 10^9$ (Poreda et al., 1992). In contrast, previous studies of off-axis regions (e.g., Vestfirðir; Hilton et al., 1998b) reveal $CO_2/^3He$ values that are generally lower than HT samples, varying by nearly 4 orders of magnitude from 4×10^6 to 3×10^{10}. Carbon systematics of the adjacent Reykjanes and Kolbeinsey ridge segments allow pre-eruptive CO_2 melt estimates 396 ± 48 ppm, and $\delta^{13}C = -3.9 \pm 1.0‰$ for the Reykjanes Ridge (de Leeuw, 2007)

and 400 ± 100 ppm, and $\delta^{13}C = -6.0 \pm 1.0‰$ for the Kolbeinsey Ridge (Macpherson et al., 2005a). Notably, these estimates are compatible with DMM source CO_2 estimates of 44 to 103 ppm Marty (2012), which would result in pre-eruptive melt CO_2 contents between 367 and 858 ppm, assuming 12% partial melting (Marty, 2012) and the highly incompatible nature of CO_2. This range also overlaps with estimates using olivine-hosted melt inclusions from the Laki fissure eruption in the ERZ of Iceland (430–510 ppm CO_2; Metrich et al., 1991).

3. SAMPLING AND ANALYTICAL TECHNIQUES

3.1. Geothermal fluids and gases

Geothermal activity is pervasive throughout Iceland with high-temperature (HT) geothermal systems (>150 °C at 1 km depth) found in the axial rift zones, and low-temperature (LT) systems (<150 °C at 1 km depth) restricted to off-axis volcanic flank zones and older regions of the Icelandic crust (Bodvarsson, 1961; Fridleifsson, 1979; Arnórsson, 1995; Arnórsson et al., 2008). In this study, both fluid and gas phase samples were collected from Icelandic neovolcanic zones, including 21 samples from the WRZ, 9 from the ERZ, 14 from the NRZ, 2 from the SIVZ and 2 from the SNVZ. In addition, 9 samples were collected in the SISZ and 14 from the Vestfirðir region of the NW Peninsula. Samples were collected over three sampling campaigns (summer 2006, 2007, and 2008) from a variety of sites, including: (a) 10 fumaroles, (b) 15 bubbling hot pools, (c) 4 water springs, (d) 4 mud pots, and (e) 15 geothermal borehole wells. Forty-eight individual localities were sampled (Fig. 1 – closed symbols), with duplicate samples collected at 23 sites, making a total of 71 geothermal samples. Fluids and gases were collected in evacuated low-He diffusivity Corning 1720-glass flasks following procedures aimed at minimizing atmospheric contamination (see Hilton, 2002 for sampling details).

In the laboratory, an ultra-high vacuum (UHV) extraction line was used to process all gas and fluid samples (see Kulongoski and Hilton, 2002 for a description of the extraction line). Following release into the UHV line, all fluid samples were acidified with phosphorus pentoxide to ensure complete release of CO_2 and, as a result, measured CO_2 abundances correspond to the total dissolved inorganic carbon (DIC) content. A glass trap held at acetone-dry ice temperature was used to isolate water vapor and a stainless-steel U-tube, held at liquid nitrogen temperature, was used to condense CO_2 and separate it from non-condensable volatiles. The light noble gases (He and Ne) were isolated using a hot (700 °C) Ti-getter and charcoal finger held at liquid nitrogen temperature, which removed active gases (N_2, CO, CH_4) and heavy noble gases (Ar, Kr and Xe), respectively. A calibrated fraction of the He and Ne gas was captured in an AR-glass breakseal for transfer to a MAP-215 noble gas mass spectrometer for He isotope analysis (see Füri et al., 2010 for measurement details). The CO_2 fraction was condensed into a Pyrex breakseal for transfer to a dedicated CO_2 cleanup line.

The CO_2 gas fraction was further purified on a separate cleanup and quantification line, constructed from Pyrex glass, whereby CO_2 was resolved from any sulfur-bearing species using a variable temperature trap. Following cleanup, the total amount of CO_2 was measured using a capacitance manometer in a calibrated volume, thus enabling the CO_2 abundance (and $CO_2/^3He$ ratios with He data from Füri et al., 2010) to be calculated. Finally, CO_2 was refrozen into a Pyrex tube for transfer to either a VG Prism mass spectrometer (2006, 2007 sampling trips) or a Thermo Finnigan Delta XP_{plus} isotope ratio mass spectrometer (2008 sampling trip) for carbon isotopic ($\delta^{13}C$) analysis. Carbon isotope $\delta^{13}C$ (CO_2) values are reported relative to the international reference standard, VPDB. Agreement between the two instruments was determined to be better than 0.5‰, by running the limestone laboratory standard (NBS-19; Friedman et al., 1982) on both mass spectrometers. Precision of individual analyses of standards and samples is better than 0.1‰; however, we estimate the accuracy of our $\delta^{13}C$ determinations (±0.5‰) by repeat analyses of NBS-19, itself calibrated relative to VPDB. Procedural blanks were processed on the extraction line and comprised less than 1% of sample abundance releases.

3.2. Subglacial basaltic glasses

We analyzed subglacial basaltic glasses collected from a total of 47 locations, divided between the WRZ ($n = 17$), ERZ ($n = 10$), NRZ ($n = 16$), SIVZ ($n = 3$), and SNVZ ($n = 1$) (Fig. 1). All subglacial basaltic glasses belong to the Móberg formation (e.g., Jakobsson and Gudmundsson, 2008), which is the general term for volcanic rocks formed during the Brunhes geomagnetic epoch at the end of the Pleistocene (0.78–0.01 Ma) (Jóhannesson and Sæmundsson, 1998). We note that most samples are fresh, which suggests relatively young formation ages (i.e., during the last glaciation). This is consistent with observations in the field, as well as cosmogenic exposure ages (Licciardi et al., 2007) that indicate formation during the last deglaciation (~15 ka). Subglacial basalts in Iceland range in composition from alkalic (off-axis), through transitional, to tholeiitic along the axial rift zones, and apart from four (off-axis) samples (i.e., RET-1, TRÍ-3, BHE-43 and OLAF-1), all our samples are tholeiitic in composition.

In the laboratory, glasses were ultrasonically cleaned in dichloromethane to remove any organic contaminants from the glass surface. Next, approximately 10–20 individual glass chips (totaling 100–300 mg), free of surficial alteration, phenocrysts, or large vesicles were handpicked using a binocular microscope. The selected glass was then ultrasonically cleaned in a 1:1 acetone–methanol mixture, dried, and transferred to a quartz-glass sample finger on the extraction line, evacuated to UHV, and held at 150 °C overnight.

Samples were analyzed for total CO_2 abundance and carbon isotope ($\delta^{13}C$) values.

Carbon was extracted from basaltic glass chips using a stepped heating method on a dedicated all-glass extraction line (after Macpherson et al., 1999). For each extraction, the temperature was incrementally raised in 100 °C steps

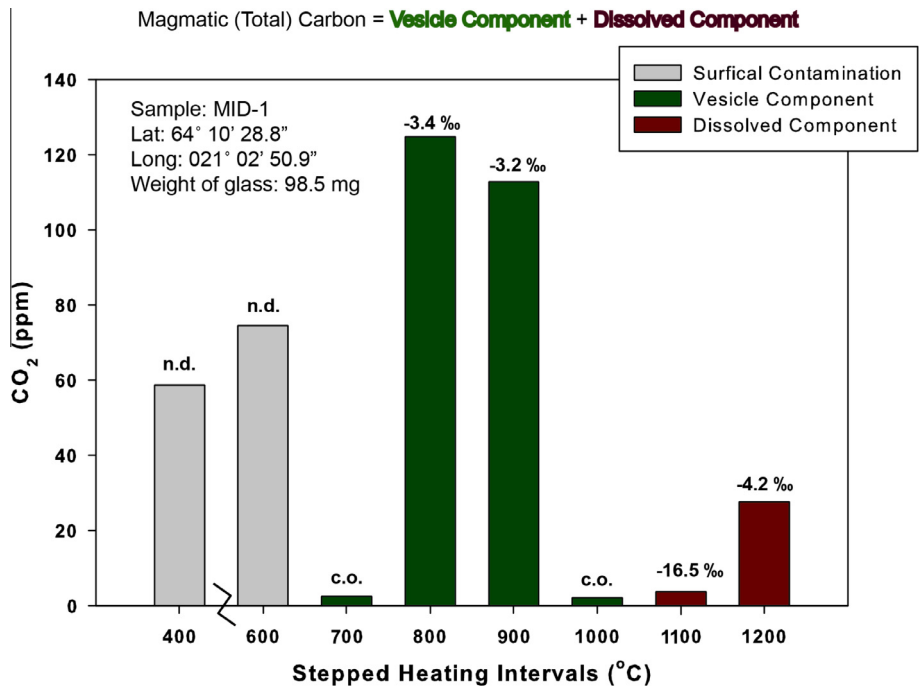

Fig. 2. Carbon content (ppm) release pattern as a function of incremental temperature step for a typical basalt sample (MID-1). CO_2 released between 400 and 600 °C is derived from surficial contamination on the glass, CO_2 released from 700 to 900 °C is derived from vesicle-cited CO_2 within the glass, and CO_2 released between 1000 and 1200 °C represents CO_2 dissolved in the melt immediately prior to quenching to form glass. Carbon isotope values are also shown for individual temperature steps. If the CO_2 yield from an individual step was too low, the CO_2 was carried over (c.o.) to the next temperature step. Carbon isotopes were not determined (n.d.) between 400 and 600 °C, as this CO_2 is considered to be unrepresentative of magmatic carbon.

from 400 °C to 1200 °C (excluding the 500 °C step), each lasting 30 min. During the first two heating steps (400 °C and 600 °C), samples were combusted in pure oxygen, generated using a CuO furnace, to remove possible C contaminants, whereas the 700–1200 °C pyrolysis steps (i.e., without oxygen) released magmatic carbon (Fig. 2). After each heating step, the CO_2 was separated from other gases (i.e., H_2O, SO_2) using a variable temperature trap cooled with liquid nitrogen. Following purification, total CO_2 abundances were measured in a calibrated volume using a Baratron™ capacitance manometer. Carbon dioxide released during the (first two) combustion steps was not collected, as this gas is expected to be dominated by secondary surface contamination acquired by the glass post-eruption (Des Marais and Moore, 1984; Mattey et al., 1984, 1989; Exley et al., 1986). However, for the 700–1200 °C steps, CO_2 was collected in Pyrex® glass tubes at each successive temperature step for subsequent isotopic ($\delta^{13}C$) analysis. Low temperature (700–900 °C) CO_2 releases are taken to represent the "vesicle" carbon (CO_2^v) component, whereas higher temperature (1000–1200 °C) releases represent the "dissolved" carbon (CO_2^d) component (Fig. 2). Whenever the CO_2 yield from a single temperature step was deemed too small (<3 ppm) for isotopic analysis, the CO_2 was combined with CO_2 released during the following step. All aliquots of CO_2 (corresponding to each temperature step) were analyzed for carbon isotopes ($\delta^{13}C$) using the mass spectrometers described above. Procedural blanks were run prior to loading samples and blank subtractions, typically comprising less than 5% of the sample release, were applied. Precision and accuracy of the basalt $\delta^{13}C$ values are the same as for geothermal fluids. In order to derive basalt $CO_2/^3He$ ratios, vesicle CO_2 contents were combined with He data obtained by crushing from Füri et al. (2010).

4. RESULTS

4.1. Geothermal fluids

We report $\delta^{13}C$ values (vs. VPDB), CO_2 abundances (for fluid phase samples) and $CO_2/^3He$ ratios for a suite of 48 geothermal samples (Table 1). Sample locations are given in Fig. 1 (closed symbols). $CO_2/^3He$ and $\delta^{13}C$ variations as a function of latitude are plotted (together with glass data) in Fig. 3A and B, respectively.

4.1.1. Geothermal carbon isotopes ($\delta^{13}C$)

Geothermal fluids and gases display carbon isotope values ranging from −18.8‰ to +4.6‰ (Fig. 3B). Axial rift zone samples span a narrower range of $\delta^{13}C$ values compared to Iceland as a whole, with WRZ values ranging from −5.1‰ to +0.5‰, ERZ from −3.7‰ to +1.6‰ and NRZ from −5.3‰ to +2.9‰. Only two $\delta^{13}C$ values were obtained in SIVZ (Seljavellir) samples, both ∼−3.4‰. Likewise, just two $\delta^{13}C$ values were determined in SNVZ (Lýsuhóll), ranging from −6.6‰ to −6.1‰. In contrast, off-axis samples extend over a much greater range, with SISZ values varying from −18.8‰ to −2.9‰, and Vestfirðir values ranging from −8.8‰ to +4.7‰ (Fig. 3B). These findings extend the previously observed range in $\delta^{13}C$ (−16‰ to

Table 1
Carbon characteristics of Icelandic geothermal fluids and gases.

Location	Latitude (N)	Longitude (W)	Sample ID[a]	Sample[b] Type	Temp. (°C)	$CO_2/^3He$[c] ($\times 10^9$)	$\delta^{13}C$‰ vs. VPDB	mmolCO_2/kg H_2O
Western Rift Zone (WRZ)								
Nesjavellir	64°05′45.6″	021°16′48.0″	ICE-1	B	240	–	0.40	–
			ICE-3	B	240	1.46	0.50	–
Nesjavellir	64°05′36.6″	021°16′28.3″	ICE08–11	G	89.0	8.62	−4.69	–
			ICE08–12	G	89.0	5.59	−2.59	–
Svartsengi	63°52′32.8″	022°26′06.6″	ICE-5	B	240	1.54	−4.23	–
			ICE-6	B	240	1.61	−3.28	–
Reykjanes	63°49′06.7″	022°41′04.7″	PBICE-1	G	100	1.67	−3.40	–
			PBICE-2	G	100	1.31	−2.99	–
Krísuvík	63°53′43.1″	022°03′19.2″	PBICE-3	G	99.6	4.25	−3.43	–
			PBICE-4*	G	99.6	1.32	−3.93	–
Krísuvík	63°53′43.1″	022°03′19.3″	ICE08–14	G	77.5	10.70	−4.23	–
			ICE08–15	G	77.5	4.79	−3.59	–
Hengill	64°01′12.1″	021°23′41.6″	PBICE-9	G	72.8	4.17	−3.96	–
			PBICE-12	G	72.8	8.24	−4.45	–
Hengill	64°00′25.0″	021°20′30.4″	ICE08–22	G	77.5	6.27	−3.10	–
Little Geysir	64°18′38.4″	020°18′08.8″	PBICE-13	G	82.6	0.63	−2.73	–
			PBICE-14	G	82.6	0.60	−2.66	–
Kerlingafjöll	64°38′37.0″	019°17′17.1″	PBICE-10	G	94.7	3.72	−4.06	–
Hveravellir	64°51′55.6″	019°33′29.7″	PBICE-11	G	89.6	0.84	−5.05	–
Hveragerði	64°01′20.1″	021°11′38.5″	PBICE-16	G	100.7	1.00	−2.36	–
			PBICE-8	G	100.7	1.97	−2.32	–
Eastern Rift Zone (ERZ)								
Landmannalaugar	63°58′52.2″	019°05′21.3″	PBICE-5*	G	98.6	2.91	−3.04	–
Landmannalaugar	63°59′32.7″	019°06′01.7″	ICE08–26*	W	99.5	1328	−2.21	1.95
Landmannalaugar	63°59′21.2″	019°06′42.1″	ICE08–29*	G	99.1	28.7	–	–
Landmannalaugar	63°59′26.8″	019°03′46.4″	ICE08–30*	W	64.9	165	–	0.19
Köldukvíslabotnar	64°34′15.2″	018°06′39.9″	ICE08–17*	B	–	1760	−3.74	2.81
			ICE08–18*	B	–	1684	−2.54	2.87
Vonarskarð	64°41′32.3″	017°53′47.5″	ICE08–16	G	97.7	14.1	1.62	–
			ICE08–21	G	97.7	7.81	1.42	–
Vonarskarð	64°41′26.8″	017°52′53.9″	ICE08–13	W	64.5	27.5	−2.48	5.52
Northern Rift Zone (NRZ)								
Krafla	65°42′16.3″	016°44′42.4″	ICE-11	B	–	4.92	−4.31	–
			ICE-12	B	–	3.98	−5.26	–
Krafla	65°42′31.4″	016°45′38.7″	ICE-10	B	–	3.8	−1.7	–
			ICE-17	B	–	6.11	−1.39	–
Krafla	65°43′18.2″	016°47′15.5″	PBICE-20	G	76.5	2.93	−4.37	–
Krafla	65°43′18.0″	016°47′15.5″	ICE08–06	G	96.7	4.58	−4.78	–
Krafla	65°43′09.9″	016°47′17.4″	ICE08–10	G	96.7	18.4	−2.44	–
Námafjall	65°38′26.9″	016°48′34.7″	ICE08–03	G	–	15.6	−5.29	–
Námafjall	65°38′26.8″	016°48′30.4″	ICE08–02	G	–	8.78	−5.09	–
Þeystareykir	65°52′23.0″	016°58′12.7″	ICE08–09	G	89.9	0.04	2.86	–
Askja, Viti crater	65°02′40.4″	016°43′31.4″	PBICE-18	G	26.8	9.12	−3.58	–
Askja, Viti crater	65°02′48.0″	016°43′29.2″	ICE08–05	G	30.5	9.43	−4.19	–
Kverkfjöll	64°40′30.1″	016°41′33.6″	ICE08–19	G	–	7.75	−2.43	–
	64°40′30.1″	016°41′33.6″	ICE08–20	G	–	34.21	−1.98	–
South Iceland Volcanic Zone (SIVZ)								
Seljavellir	63°33′56.1″	019°36′31.1″	ICE-8	B	50.0	0.491	−3.37	3.53
			ICE-9	B	50.0	0.648	−3.44	3.45
Snæfellsnes Volcanic Zone (SNVZ)								
Lýsuhóll	64°50′40.7″	023°13′10.6″	ICE-18	B	–	2.42	−6.61	–
			ICE-7	B	–	2.41	−6.07	–
South Iceland Seismic Zone (SISZ)								
Hæðarendi	64°04′31.8″	020°51′36.3″	ICE-21	B	–	–	−3.47	–
			ICE-22	B	–	0.974	−4.52	–

(*continued on next page*)

Table 1 (*continued*)

Selfoss	63°56′46.3″	020°57′38.3″	PBICE-17	B	70.0	0.025	−18.8	–
			PBICE-19	B	70.0	0.021	−17.9	–
Þjórsárdalslaug	64°09′41.7″	019°48′41.4″	ICE08–27	G	70.0	0.00001	−10.5	–
			ICE08–28	G	70.0	0.00002	−11	–
Flúðir	64°07′45.3″	020°19′25.0″	ICE08–23	B	–	1.17	−6.13	1.02
Ormsstaðir	64°02′29.9″	020°39′46.3″	ICE08–25	B	86.9	0.08	−5.89	0.35
Eyvik	64°02′48.4″	020°41′59.4″	ICE08–24	B	73.5	0.025	−2.88	3.02
Vestfirðir (NW Peninsula)								
Hveravik	65°41′54.1″	021°33′35.2″	ICE-23	W	76.7	0.405	−3.79	0.81
			ICE-24	W	76.7	0.226	–	0.53
Laugarhóll	65°46′51.5″	021°31′13.2″	ICE-25*	G	40.2	0.001	–	–
			ICE-26*	G	40.2	0.002	–	–
Goðdalur	65°49′39.8″	021°35′30.2″	ICE-28	W	55.9	1.84	–	0.38
Gjögur	66°00′01.7″	021°19′12.5″	ICE-29	G	28.6	0.0002	–	–
			ICE-30	W	71.6	0.59	4.57	0.28
Krossnes	66°03′01.7″	021°30′22.5″	ICE-31	G	60.0	0.00008	–	–
			ICE-33	G	60.0	0.00002	–	–
Laugaland	66°01′11.7″	022°23′43.8″	ICE-34*	G	48.8	0.0007	–	–
Heyardalur	65°50′23.0″	022° 40′39.9″	ICE-36	W	44.4	0.981	−8.81	0.35
Laugar, Orkubú Vestfjarðá	66°06′40.6″	023°27′17.4″	ICE-37	B	66.0	0.041	−3.84	0.29
Laugardalsá	65°39′23.0″	023°54′36.7″	ICE-38	W	–	0.157	−5.11	0.33
Reykhólar	65°27′15.8″	022°11′52.7″	ICE-39	B	95.0	2.78	−5.49	0.42

Samples denoted with a (*) are considered to be air-contaminated based on $^4He/^{20}Ne$ and $^3He/^4He$ values (see Füri et al., 2010 for details).
[a] Samples labeled ICE-X, PBICE-X, and ICE08-X were collected in 2006, 2007, or 2008, respectively.
[b] Samples are designated: G = gas, W = water, and B = collected from a borehole.
[c] Calculated using the total CO_2, He and $^3He/^4He$ (from Füri et al., 2010).

−6‰; Hilton et al., 1998b) to higher values for the Vestfirðir region. The lowest $\delta^{13}C$ value of the present study is from the Selfoss region of the SISZ (−18.8‰), and the highest value is from a bubbling pool in Gjögur, Vestfirðir (+4.6‰) (Fig. 3B). The observation that off-axis samples display a significantly greater range in $\delta^{13}C$ values suggests that they are more susceptible to modification than axial rift zone samples (see Section 5.1). The mean $\delta^{13}C$ value for all geothermal samples is -4.0 ± 3.7‰; however, if only axial rift zone (i.e., WRZ, ERZ, NRZ) samples are considered then the average value increases to -3.1 ± 1.9‰. These values are in good agreement with previous results (Poreda et al., 1992), who reported an average $\delta^{13}C$ value of -3.8 ± 0.7‰ for a more limited dataset of HT samples (n = 8) from the axial rift zones (i.e., WRZ, ERZ, and NRZ).

4.1.2. Geothermal abundance characteristics and $CO_2/^3He$

Abundances of CO_2 were calculated for all 18 fluid phase samples, with concentrations ranging between 0.28 and 5.52 mmolCO_2/kg H_2O (Table 1 and Fig. 4B and D). Generally, neovolcanic samples displayed higher CO_2 abundances, ranging from 1.95 to 5.52 mmolCO_2/kg H_2O compared to off-axis samples, which range from 0.28 to 3.02 mmolCO_2/kg H_2O (see Fig. 4B and D). The present samples span a greater range in [CO_2] than previously reported (e.g., 0.06–1.24 mmolCO_2/kg H_2O; Poreda et al., 1992).

The ratio of CO_2 to He (reported as $CO_2/^3He$) for geothermal fluids and gases is obtained by combining previously reported $^3He/^4He$ values and total helium contents of the present sample suite (Füri et al., 2010) with carbon concentrations (this work). For Iceland as a whole, $CO_2/^3He$ values vary over 8 orders of magnitude, from 1×10^4 to 2×10^{12} (Fig. 3A). Geothermal samples from the neovolcanic zones are less variable, ranging from 4×10^7 to 2×10^{12} (Table 1), with WRZ values spanning values from 6×10^8 to 1×10^{10}, ERZ from 3×10^9 to 2×10^{12}, NRZ from 4×10^7 to 3×10^{10}, SIVZ from 5–6 $\times 10^8$, and at SNVZ both values are $\sim 2 \times 10^9$ (Fig. 3A – black symbols). In contrast, samples from older portions of the crust (i.e., SISZ and Vestfirðir) extend to significantly lower values, with a range in the SISZ from 1×10^4 to 1×10^9 and in Vestfirðir from 2×10^4 to 3×10^9 (Fig. 3A – grey symbols).

4.2. Basalts

Carbon dioxide concentrations and isotopic ratios ($\delta^{13}C$) were measured for 47 fresh subglacial basalts, which had been characterized previously for He–Ne–Ar abundances and isotope systematics (Füri et al., 2010). Sample locations are provided in Fig. 1 (open symbols) and magmatic $CO_2/^3He$ and $\delta^{13}C$ variations are plotted as a function of latitude (°N), along with geothermal values, in Fig. 3A and B, respectively.

4.2.1. Basalt carbon isotopes ($\delta^{13}C$)

Basalt carbon isotopic data using the stepped heating technique are given in Table S1 and summarized in Table 2. Vesicle $\delta^{13}C^v$ values range from −26.7‰ to −3.3‰, with an average value of -14.9 ± 5.9‰, whereas dissolved $\delta^{13}C^d$ values range from −27.5‰ to −3.3‰, with an average value of -12.4 ± 6.4‰. Total magmatic carbon (weighted

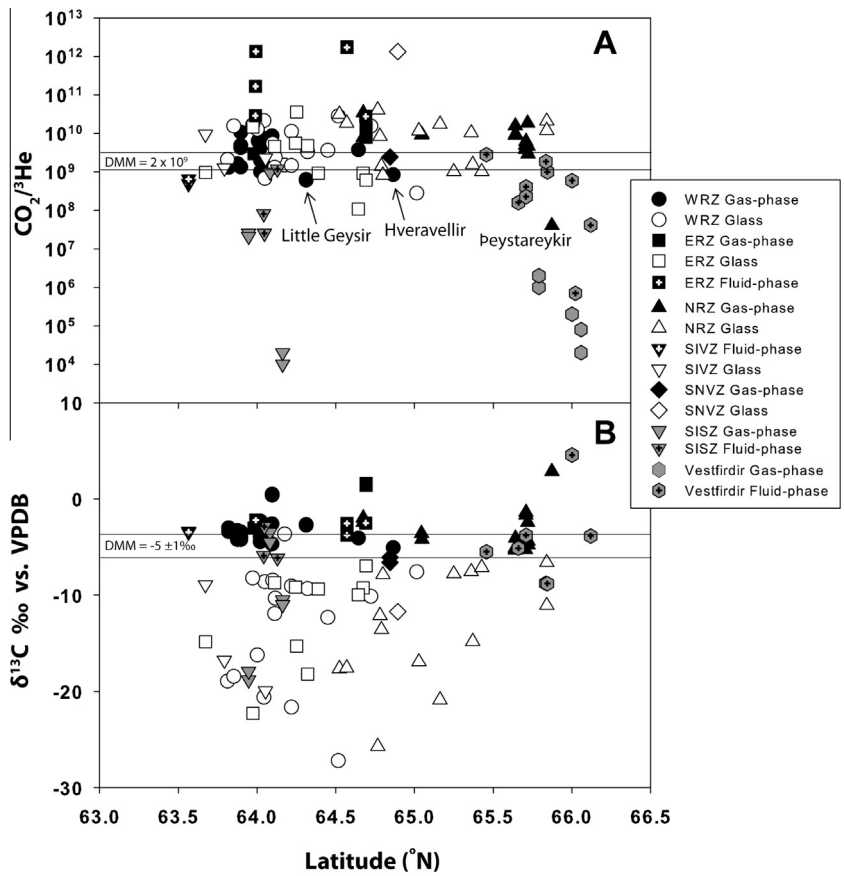

Fig. 3. $CO_2/^3He$ values (A) and carbon isotopes $\delta^{13}C$ (B) as a function of latitude for geothermal fluids/gases and subglacial basalts of Iceland. Neovolcanic zone gas samples are show as black symbols and off-axis gas samples are represented by grey shaded symbols. Fluid samples are denoted with crosses. Subglacial basalt samples are represented with open symbols. DMM ranges for $CO_2/^3He$ and $\delta^{13}C$ from Marty and Jambon (1987), and Marty and Zimmermann (1999) and Cartigny (2005), respectively.

average of vesicle and dissolved components) ranges from −27.2‰ to −3.6‰, with an average value of -13.3 ± 5.8 (Fig. 3B).

4.2.2. Basalt CO_2 abundance characteristics and $CO_2/^3He$

Carbon dioxide contents of Iceland basalts are shown in Fig. 5, which plots CO_2^v vs. CO_2^d, along with CO_2 contents of basalts from the Reykjanes and Kolbeinsey ridges (Macpherson et al., 2005a; de Leeuw, 2007). Approximately one half of the Iceland samples fall below/above the 1:1 line, indicating that, on average, the total magmatic carbon (CO_2^m) is distributed evenly between vesicle and glass phases. However, it is important to point out that CO_2 contents in subglacial basalts of Iceland are exceptionally low (typically ≪100 ppm; this work) compared to typical ocean basalts (367–858 ppm; Marty, 2012) and basalts collected along the adjacent ridges (Macpherson et al., 2005a; de Leeuw, 2007).

By combining previously published helium isotope ($^3He/^4He$) and abundance data (Füri et al., 2010) with vesicle CO_2 contents (this work), we calculate $CO_2/^3He$ values for the present sample suite. The total range of $CO_2/^3He$ values extends from 1×10^8 to 1×10^{12}. WRZ samples vary from 3×10^8 to 3×10^{10}, ERZ range from 1×10^8 to 4×10^{10}, NRZ from 8×10^8 to 7×10^{11}, SIVZ from 1–9 ($\times 10^9$) and at SNVZ the only value is 1×10^{12} (Fig. 3A – open symbols). The mean $CO_2/^3He$ value of axial rift zone basalts is 24 ± 99 ($\times 10^9$). Notably, no basalts were collected in the older portions of the crust (i.e., SISZ and Vestfirðir) due to the lack of fresh glasses. These results, together with geothermal data, expand the CO_2 database for Iceland and demonstrate that the range in CO_2 characteristics, including $CO_2/^3He$, is much broader than previously reported (Poreda et al., 1992).

5. DISCUSSION

In this section, we identify geothermal and subglacial basalt samples that display carbon isotope and abundance characteristics that are likely representative of the Icelandic mantle source vs. samples whose carbon characteristics have been compromised by secondary processes. Geothermal and basalt samples are dealt with separately as they are subject to different modification processes. After identifying unmodified samples, we demonstrate how intrinsic mantle source carbon characteristics can be determined and used to estimate carbon fluxes from the Icelandic mantle.

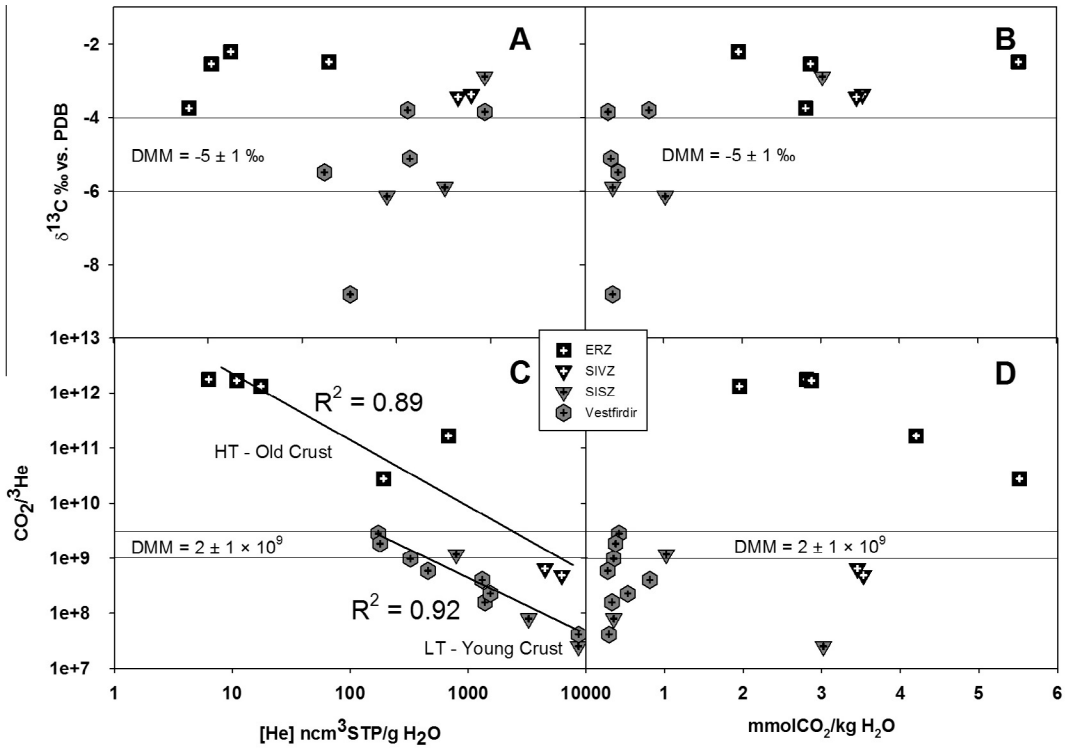

Fig. 4. Carbon isotope $\delta^{13}C$ (A and B) and $CO_2/^3He$ (C and D) values as a function of the [He] and [CO_2] content of fluid samples from younger neovolcanic zones (black symbols) and older off-axis areas of the Iceland crust (grey symbols). Panel C highlights the two regions (old vs. young crust) in terms of $CO_2/^3He$ and [He] characteristics. There is a broad negative correlation ($R^2 = 0.92$ and 0.89 for young and old regions, respectively) between $CO_2/^3He$ and [He] content. Note that off-axis samples (grey) are marked by low CO_2 and low $CO_2/^3He$ values (Panel D) suggesting CO_2 loss in older, LT geothermal systems in older regions of the Icelandic crust.

5.1. Geothermal sample integrity and modification

There are a number of processes that can modify magmatic volatile signatures, both within magmatic systems and during transport to the surface by aqueous fluids. An example of the former is magma degassing, which can modify the $CO_2/^3He$ characteristics of melts and, consequently, glasses due to solubility differences between CO_2 and He in parental melts (Hilton et al., 1998a). In the latter case, (1) phase-separation and degassing (e.g., vapor/steam separation and/or gas exsolution) can significantly alter $CO_2/^3He$ due to solubility differences between CO_2 and He in aqueous fluids (e.g., Weiss, 1971; Dubacq et al., 2013), and (2) CO_2 sequestration resulting from calcite precipitation, can modify $CO_2/^3He$ values. Furthermore, these processes can also significantly fractionate the carbon isotopes (Ray et al., 2009; Barry et al., 2013). To assess these various possibilities, we investigate both regional (i.e., latitudinal) variations in $\delta^{13}C$ and $CO_2/^3He$ (Fig. 3), as well as relationships between fluid chemistry (i.e., volatile contents), $\delta^{13}C$, and $CO_2/^3He$ (Fig. 4).

5.1.1. Pre-eruptive magma degassing

Degassing of volatiles from a tholeiitic melt can induce fractionation between various species due to solubility differences in the melt phase. For example, the solubility of He (6.4×10^{-4} cm^3 STP/g) and CO_2 (2.7×10^{-4} cm^3 STP/g) acts to lower $CO_2/^3He$ ratios of residual gases in the melt phase following degassing relative to initial starting values (Hilton et al., 1998a). In deciding whether observed $CO_2/^3He$ ratios in Icelandic geothermal systems could represent either intrinsic source values or fractionated ratios, the key consideration is knowledge of the starting $CO_2/^3He$ ratio of the Icelandic mantle.

Various tectonic settings, both globally and within Iceland, have been well-characterized for their $CO_2/^3He$ characteristics. For example, (1) the canonical upper mantle (DMM) $CO_2/^3He$ value is $\sim 2 \pm 1 \times 10^9$ (Marty and Jambon, 1987); (2) the Icelandic mantle $CO_2/^3He$ value ranges from ~ 3 to 6×10^9 (Poreda et al., 1992); (3) the adjacent Kolbeinsey and Reykjanes ridges are marked by $CO_2/^3He$ values of 2×10^9 (Macpherson et al., 2005a) and $<1 \times 10^9$ (de Leeuw, 2007), respectively; (4) High-$^3He/^4He$ (mantle) plumes have $CO_2/^3He$ values generally higher than DMM (Marty and Tolstikhin, 1998; Shaw et al., 2004) despite the fact that theoretical estimates of volatile contents of the lower mantle source region (e.g., Porcelli and Wasserburg, 1995; Javoy, 1997) predict a value of $\sim 2 \times 10^8$, which would be more consistent with $CO_2/^3He$ values in some meteorite-types (i.e., E-chondrites; Marty and Zimmermann, 1999).

$CO_2/^3He$ ratios were determined for a total of 43 axial rift zone gas and fluid samples. Assuming DMM-like starting $CO_2/^3He$ and $\delta^{13}C$ compositions of $2 \pm 1 \times 10^9$ and -5 ± 1‰, respectively (Marty and Jambon, 1987; Marty and Zimmermann, 1999; Cartigny, 2005), we note that only

3 axial rift zone samples have $CO_2/^3He$ values below this canonical range: Little Geysir = $\sim 6 \times 10^8$, Hveravellir = 8×10^8 and Þeystareykir = 4×10^7 (Fig. 3A). In this respect, pre-eruptive degassing seems to affect very few axial rift zone gas and fluid samples. Alternatively, if high $^3He/^4He$ oceanic mantle is accompanied by greater than DMM-like $CO_2/^3He$ values (Poreda et al., 1992; Marty and Tolstikhin, 1998) then secondary modification (i.e., lowering $CO_2/^3He$ values) would have to be pervasive throughout Iceland. The preponderance of DMM-like $CO_2/^3He$ ratios along adjacent ridges suggests that such a $CO_2/^3He$ starting composition could be justified for Iceland and, consequently, that magma degassing has not significantly affected measured $CO_2/^3He$ values of geothermal fluids.

In contrast to rift axis samples, the majority of off-axis fluid samples display $CO_2/^3He$ significantly below the DMM threshold, suggesting either a much different degassing history involving extensive volatile loss and/or an extensive secondary modification process (e.g., calcite precipitation; see Section 5.1.3), which has modified the majority of off-axis geothermal samples. If a DMM-like starting $CO_2/^3He$ value is indeed adopted, then the minimum possible $CO_2/^3He$ value achievable by closed system degassing is 5.5×10^8 (i.e., $2 \times 10^9/\alpha$; where the fractionation factor (α) between He and CO_2 = $\sim$2.35, expressed as the inverse ratio of their solubilities (Hilton et al., 1998a). Similarly, carbon isotopes are expected to fractionate according to the experimentally-derived isotope fractionation of carbon between CO_2 and carbon dissolved in a tholeiitic magma ($\delta^{13}C$ fractionation factor = $\Delta = -4‰$; Javoy et al., 1978; see Mattey, 1991 compilation), resulting in a corresponding $\delta^{13}C$ value of $-10.5‰$. Therefore the low $CO_2/^3He$ values observed at Little Geysir and Hveravellir could potentially be explained by closed system degassing; however, addition of high $\delta^{13}C$ carbon would then be necessary to explain the correspondingly high (>DMM) carbon isotope values of other samples. Alternatively, if open system (Rayleigh) degassing occurred, then extremely low $CO_2/^3He$ and $\delta^{13}C$ values could potentially be achieved, depending on the fraction of volatile loss; however, no geothermal samples are marked by such low carbon isotope values ($<-20‰$) and therefore open system degassing is considered highly unlikely.

5.1.2. Hydrothermal phase partitioning

In addition to magmatic degassing processes, fractionation between CO_2 and He can also occur due to solubility (S) differences in aqueous fluids (e.g., $S_{CO_2} \ll S_{He}$) (Ellis and Golding, 1963; Weiss, 1971; Dubacq et al., 2013). Helium preferentially partitions into an exsolved vapor phase relative to CO_2, leaving residual fluid-phase $CO_2/^3He$ values elevated compared to starting values. The effects of hydrothermal phase partitioning on He–CO_2 characteristics can be observed by plotting $\delta^{13}C$ and $CO_2/^3He$ as a function of volatile content (e.g., [He]; [CO_2]; Fig. 4). Fig. 4A plots carbon isotopes as a function of helium concentration $[He]_C$ (ncm^3 STP/g H_2O) and shows that HT samples have slightly higher carbon isotope ratios than LT localities. In Fig. 4C, we plot $CO_2/^3He$ vs. $[He]_C$, and we note that LT and HT samples cluster into two distinct groups: (1) LT samples are relatively He-rich and display $CO_2/^3He$ values that extend from the DMM range ($2 \pm 1 \times 10^9$) to lower values ($\sim 10^7$) at high [He], (2) HT neovolcanic zone samples have overlapping but generally lower He contents accompanied by considerably higher $CO_2/^3He$ values, extending from below the DMM range to values $>10^{12}$. For example, the most He depleted (<20 $[He]_C$ ncm^3 STP/g H_2O) samples are from the ERZ and also display the highest measured $CO_2/^3He$ values. Overall, there is a broad inverse correlation for both LT ($R^2 = 0.92$) and HT ($R^2 = 0.89$) samples (Fig. 4C). Similar observations between $CO_2/^3He$ and [He] in geothermal fluids were previously attributed to the effects of vapor-fluid partitioning, resulting in high $CO_2/^3He$ values and corresponding low He contents in residual (water) phase samples (e.g., van Soest et al., 1998; Barry et al., 2013). By again assuming a DMM-like starting value (see Section 5.1.1), we note that only ERZ fluid samples display $CO_2/^3He$ values above the canonical DMM range ($2 \pm 1 \times 10^9$), suggesting hydrothermal phase partitioning is the principal modification mechanism in this region, but most likely a relatively minor factor in LT regions such as the SISZ and Vestfirðir where $CO_2/^3He$ values are generally much lower. All ERZ $CO_2/^3He$ results plot above both the DMM $CO_2/^3He$ range and the average Icelandic plume value ($\sim 6 \times 10^9$) measured previously in the axial rift zones (Poreda et al., 1992). In contrast, LT off-axis $CO_2/^3He$ values predominantly fall below the MORB range (Fig. 4C) – particularly gas samples, which are relatively CO_2 depleted compared to fluid phase samples. These results suggest an additional process may act to lower $CO_2/^3He$ values in LT regions.

5.1.3. Calcite precipitation

The loss of CO_2 due to calcite precipitation has the potential to fractionate both $CO_2/^3He$ and carbon isotope values. Basalts have abundant magnesium- and calcium-rich silicate minerals (e.g., olivine, plagioclase), and therefore deep circulating fluids within the geothermal system are enriched in Na^+, Ca^{2+}, Mg^{2+} ions (Gysi and Stefánsson, 2012). Magmatic degassing creates low-pH, CO_2-rich fluids and gases that react with these ions to precipitate carbonate minerals according to the following reaction:

$$(Ca^{2+}, Mg^{2+}) + CO_2 + H_2O = (Ca, Mg)CO_3 + 2H^+ \quad (1)$$

During this reaction, calcite forms within the basaltic crust, which leads to lower $CO_2/^3He$ ratios in residual fluids compared to initial magmatic values.

Off-axis LT samples generally display $CO_2/^3He$ values below the DMM and/or plume-mantle range (see Section 5.1.1), extending to values as low as 1×10^4, while most axial rift zone samples fall within or slightly above the DMM range (Fig. 3A). Lower $CO_2/^3He$ values in off-axis samples vs. on-axis samples suggest preferential CO_2 loss due to calcite precipitation in older, LT portions of the crust. Fig. 4 demonstrates the fractionation effect of CO_2 loss by plotting $\delta^{13}C$ (Fig. 4B) and $CO_2/^3He$ (Fig. 4D) vs. [CO_2] content of fluid samples. Notably, the most CO_2 depleted samples occur in off-axis regions of the Icelandic crust (e.g., SISZ and Vestfirðir) and display

the lowest $CO_2/^3He$ and $\delta^{13}C$ values in Iceland. Thus, based on extremely low absolute CO_2 concentration data and low $CO_2/^3He$ values relative to assumed starting compositions, we conclude that calcite precipitation is likely the controlling process in older, LT off-axis portions of the crust. These findings are consistent with those of Hilton et al. (1998b) who showed previously that the CO_2 inventory in Vestfirðir is primarily controlled by reactions that form calcite. In this respect, we suggest that carbon removal due to calcite precipitation may be a widespread process occurring throughout the off-axis portions of Iceland.

Carbon isotope fractionation associated with calcite precipitation is highly temperature-dependent: at relatively low temperatures (<192 °C), calcite is enriched in ^{13}C relative to residual dissolved CO_2 in geothermal fluids whereas at higher temperatures (>192 °C) the fractionation is in the opposite sense (Bottinga, 1969; Hoefs, 2010). Fig. 3B shows that off-axis gas samples from SISZ display the lowest $\delta^{13}C$ values (−18.8‰). These extremely fractionated samples can be explained by calcite precipitation at calculated temperatures between 120 °C (Selfoss) and 180 °C (Þjórsárdalslaug) (Bottinga, 1969; Hoefs, 2010). In the same way, samples with low $CO_2/^3He$ and high $\delta^{13}C$ (e.g., Þeystareykir; NRZ) can be explained by calcite precipitation at ~260 °C. Notably, Selfoss and Þjórsárdalslaug samples were collected at discharge temperatures of ~70 °C, whereas Þeystareykir was sampled at ~90 °C. However, reported discharge temperatures represent minimum estimates only of reservoir temperatures. For example, borehole values of 120 °C were measured at a depth of ~1400 m in Selfoss (Arnórsson, 1995) and geothermometers suggest an average reservoir temperature of 240–300 °C in the Þeystareykir area (Armannsson et al., 1986) – both estimates are in agreement with predicted reservoir temperatures based on temperature dependent calcite precipitation (this study).

The average geothermal carbon isotope composition for all (HT and LT) fluid/gas samples (−4.0 ± 3.7‰; this study) is in good agreement with previously reported estimates of −3.8 ± 0.7‰ (Poreda et al., 1992) for CO_2-rich HT fluids of the Icelandic axial rift zones. For comparison, some hotspots (e.g., Kilauea and Society Islands) display $\delta^{13}C$ values between −3‰ and −4‰ (Gerlach and Taylor, 1990; Hilton et al., 1997; Aubaud et al., 2005), which are ^{13}C-enriched relative to DMM. In contrast, the $\delta^{13}C$ value of Loihi tholeiites is ~−6‰ (Exley et al., 1986), as are basalt estimates from the Pitcairn hotspot (~−6‰; Aubaud et al., 2006).

Following a systematic evaluation of modification processes, extreme values can be identified and removed from further consideration. For example, if LT off-axis samples affected by calcite precipitation are removed and only HT axial rift zone gas samples are considered, then the average $\delta^{13}C$ value increases to −3.1 ± 1.9‰. Significantly, this value overlaps with plume-derived values previously observed in Kilauea and the Society Islands, as well as the upper limit of the DMM range (−5 ± 1‰; Marty and Zimmermann, 1999; Cartigny, 2005), suggesting that $\delta^{13}C$ is not a sensitive discriminator between plume and DMM mantle sources, as is the case with He isotopes.

5.2. CO_2 evolution of basaltic magmas

Magma hosts CO_2 in two forms: (1) CO_2 dissolved in the melt, and (2) CO_2 exsolved into a separate vapor phase. By investigating both the dissolved (glass-matrix) and vapor (vesicle) phases in lavas, it is possible to constrain the degassing history of individual Icelandic magma batches, identify crustal assimilation processes and ultimately estimate intrinsic carbon characteristics (isotope and abundance) of the underlying mantle source (Macpherson and Mattey, 1994; Macpherson et al., 2010). Measured carbon signatures result from primary mantle source features and superimposed secondary features such as degassing and crustal assimilation. The loss of CO_2 from a basaltic magma (i.e., degassing) can potentially lower both $CO_2/^3He$ (Hilton et al., 1998a) and $\delta^{13}C$ values (Javoy et al., 1978; Mattey, 1991) in the residual melt phase. In addition, crustal assimilation and/or contamination can further modify source features due to mixing with isotopically-distinct crustal components (Macpherson et al., 2010). Thus, before primary basalt carbon characteristics can be identified, the effects of the aforementioned modification processes need to be evaluated.

5.2.1. Dissolved volatiles: isotopic evolution of dissolved CO_2

The solubility of CO_2 in basaltic melts is pressure-dependent and, as a result, lavas erupted under greater confining pressures (e.g., thick glacial cover) retain higher proportions of their primary CO_2 inventory. During magma ascent, CO_2 is degassed from the melt (Bottinga and Javoy, 1990) and, due to the lower solubility of CO_2 vs. other major volatiles (e.g., H_2O), forms the principal constituent of the vapor-phase in melts (Mysen et al., 1975; Moore et al., 1977; Delaney et al., 1978; Stolper and Holloway, 1988), serving as a carrier gas for other volatile species (e.g., the noble gases). Such gas loss causes isotopic exchange amongst CO_2 partitioned between the vapor phase (vesicles = CO_2^v) and residual CO_2 (dissolved = CO_2^d) in the magma (Pineau et al., 1976; Javoy et al., 1978). Consequently, variations in CO_2 content and $\delta^{13}C$ values can be used to constrain the extent of degassing within a given magmatic system.

Degassing of CO_2 can occur in either open or closed system modes (Gerlach and Taylor, 1990; Dixon and Stolper, 1995) or as a combination (two-stage) of both mechanisms (Gerlach and Taylor, 1990; Macpherson and Mattey, 1994; Shaw et al., 2004; Macpherson et al., 2005a). In a closed system, batch equilibrium degassing (BED) occurs, whereby vesicles form in a rising melt and subsequently stay in contact with the melt, thereby facilitating continuous isotopic exchange (Macpherson and Mattey, 1994). In contrast, Rayleigh (open system) distillation or fractional equilibrium degassing (FED) takes place when vesicles form in equilibrium with the surrounding melt but are removed, as degassing progresses, due to the open nature of the system. The extent to which $^{13}CO_2$ fractionates from $^{12}CO_2$ is dependent on the fractionation factor (i.e., Δ-values) between CO_2 dissolved as carbonate ions in basaltic melt (Fine and Stolper, 1986) and free CO_2 in the vapor phase. Experimentally determined Δ-values ($=\delta^{13}C^v - \delta^{13}C^d$)

range from +2.3‰ to +4.6‰ (Javoy et al., 1978; see Mattey, 1991 compilation) and predict lower $\delta^{13}C$ values in dissolved CO_2 relative to the exsolved (vesicle) phase.

In this study, approximately two-thirds of samples (i.e., 31 of 47; Table 2) have $\delta^{13}C^d > \delta^{13}C^v$ resulting in negative Δ-values, demonstrating that melt and gas phases from the same glass are not in carbon isotopic equilibrium and that equilibrium degassing conditions do not prevail. Alternative explanations include (1) gases being derived from degassing from elsewhere within the magmatic system (Shaw et al., 2004; Hahm et al., 2012), (2) $\delta^{13}C$ values being modified by assimilation with an isotopically-distinct crustal component (e.g., Macpherson et al., 2010), and/or (3) disequilibrium degassing (Füri et al., 2010). However, prior to considering these more complicated alternative scenarios, we first adopt a basic equilibrium degassing model to describe gas loss in the simplest of terms. If we assume equilibrium degassing, then the minimum $\delta^{13}C$ value attainable in a BED system is equal to [$\delta^{13}C_{initial}$ – the fractionation factor ($\Delta_{vapor\text{-}melt}$)], whereas in a FED system any $\delta^{13}C$ value below the initial $\delta^{13}C$ value is possible. Consequently, dissolved $\delta^{13}C$ values in magmas that experienced FED degassing are typically more fractionated (i.e., to lower values) for a given degree of gas loss compared to BED degassing (Macpherson and Mattey, 1994). By considering the dissolved carbon contents and carbon isotope signatures of basalts, we can model the degassing evolution of basalts and estimate initial mantle starting compositions.

5.2.2. Equilibrium degassing modeling

Using an equilibrium degassing model (after Macpherson and Mattey, 1994), pre-eruptive carbon characteristics (e.g., CO_2 contents and $\delta^{13}C$ values) of Iceland subglacial basalts can be estimated. Importantly, this type of model assumes: (1) samples are derived from a distinct parental melt composition, (2) a common fractionation factor ($\Delta_{vapor\text{-}melt}$) of ~4.2 (defined by the FED trajectory – see below) is appropriate for all samples, (3) degassing alone (FED and/or BED) is solely responsible for all $\delta^{13}C$ variability unless otherwise indicated, and (4) samples which fall on or within the envelope defined by the FED and BED trajectories result from BED, FED or a combination (two stage degassing) of the two processes.

Due to the complicated effects of melt generation and source heterogeneities in the Icelandic mantle (Slater et al., 1998; Thirlwall et al., 2004; Stracke and Bourdon, 2009; Füri et al., 2010), the Icelandic source of basalt CO_2 may not be characterized by a single source composition, as was assumed in previous studies which employed this type of degassing model (Macpherson and Mattey, 1994; Shaw et al., 2004; Macpherson et al., 2005a). In order to circumvent this potential problem, CO_2 estimates are made for individual rift zone segments (i.e., WRZ, ERZ, NRZ; Fig. 6A–C) as well as for Iceland as a whole (Fig. 6D and E). In this way, the CO_2 (isotope and concentration) characteristics of Iceland basalts can be best explained by degassing of several distinct pre-eruptive melts.

Initial CO_2 contents and $\delta^{13}C$ values of the magma source prior to degassing are estimated using the following equations (after Macpherson and Mattey, 1994):

$$\delta_r BED = \delta_p - \Delta(1 - (C_r BED/C_p)) \quad (2)$$

$$\delta_r FED = \delta_p + \Delta(\ln(C_r FED/C_p)) \quad (3)$$

where δ_rBED and δ_rFED represent the isotopic composition ($\delta^{13}C$) of CO_2 remaining dissolved in the melt following BED and FED, C_rBED and C_rFED are the residual concentrations of CO_2 for BED and FED, C_p and δ_p represent pre-eruptive (initial) concentration and isotopic composition of CO_2 dissolved in the melt prior to BED and FED, and $\Delta = \delta^{13}C_{vapor} - \delta^{13}C_{melt}$, which is empirically calculated for each individual rift zone. Due to the fact that one δ_r value corresponds to two residual CO_2 concentrations (C_rBED and C_rFED) for the two types of degassing (BED and FED), the two above equations can be combined:

$$\ln C_p + (C_r BED/C_p) = 1 + \ln C_r FED \quad (4)$$

and C_p can then be calculated using C_rBED and C_rFED values corresponding to two different residual isotopic compositions ($\delta_r 1$ and $\delta_r 2$), using:

$$C_p = \left(C_r BED^1 - C_r BED^2\right) / \ln\left(C_r FED^1 / C_r FED^2\right) \quad (5)$$

Using this approach, we can assess the possibility of CO_2 heterogeneities in pre-eruptive melts (prior to degassing) between the various neovolcanic rift zones of Iceland.

We begin by considering WRZ samples only, where CO_2 characteristics were determined in 17 basaltic glasses, which display a wide range in $\delta^{13}C^d$ and CO_2^d contents (Table 2). A fractionation factor of (Δ=) ~4.3 is determined for the WRZ by calculating the slope of a best fit regression line through samples SKARD-1 and MID-3, which are considered to represent a FED trajectory (see Fig. 6A). We then selected samples A-9 ($C^1_{rBED} = 42.1$ ppm, $\delta^1_r = -6.9‰$) and MAE-1 ($C^2_{rBED} = 13.3$ ppm, $\delta^2_r = -7.5‰$), which follow a BED trajectory, and calculate $C_r FED^1$ and $C_r FED^2$ using the FED regression line ($\delta_r = 4.30\ \ln(C_{rFED}) - 27.92$) that defines the Δ-value for both the BED and FED trajectories. With $C_r BED^1$ and $C_r FED^1$ and $C_r BED^2$ and $C_r FED^2$, we are able to estimate C_p using Eq. (5) and $\delta_p BED^1$, $\delta_p BED^2$, $\delta_p FED^1$, and $\delta_p FED^2$ using Eqs. (2) and (3), respectively. The estimated CO_2 composition of pre-eruptive melt is (C_p) = 206 ± 24 ppm, with a corresponding average $\delta_p = -4.2 \pm 0.9‰$ (i.e., average and standard deviation of $\delta_p BED^1$, $\delta_p BED^2$, $\delta_p FED^1$, and $\delta_p FED^2$). The degree of uncertainty associated with the C_p estimate is approximated by considering that the overall precision associated with individual $\delta^{13}C$ measurements is ± 0.5‰, based on repeat analyses of internal standards. By assuming that the same uncertainty would apply to the empirically-derived FED relationship of $\delta_r = 4.30\ \ln(C_{rFED}) - 27.92$, and thus the Δ-value, then the lower extreme of Δ = 4.3–0.5 = 3.8‰ and produces a C_p value of 182 ppm whereas the higher estimate of Δ = 4.3 + 0.5 = 4.8‰ yields a C_p estimate of 230 ppm. If our models are correct (i.e., assuming that the samples used to define Δ did not assimilate any crustal carbon and that all samples analysed degassed from the same starting concentration and isotopic compositions), then the analytical uncertainty on C_p for the WRZ is ± 24 ppm (i.e., ~12%). If these assumptions hold true for all rift segments, then the observation that all

Table 2
Carbon characteristics of Icelandic subglacial basaltic glasses[*].

Location	Latitude (N)	Longitude (W)	Sample ID	Vesicle CO_2 (ppm)[a]	Vesicle CO_2 $\delta^{13}C^{v}$	Dissolved CO_2 (ppm)[b]	Dissolved CO_2 $\delta^{13}C$	Total CO_2 (ppm)[c]	Total CO_2 $\delta^{13}C$	$CO_2/^3He$ ($\times 10^9$)	$CO_2/^3He$ corrected ($\times 10^9$)[d]
Western Rift Zone (WRZ)											
Skarðsmýrarfjall	64°02′37.6″	021°21′29.9″	SKARD-1	7	−26.5	12.1	−17.2	19.1	−20.6	21.7	–
Vífilsfell	64°02′55.4″	021°32′24.8″	VIF-1	1.1	n.d.	18.6	−8.6	19.6	−8.6	0.7	0.6
Miðfell	64°10′28.9″	021°02′50.9″	MID-1	242.1	−3.3	31.2	−6.3	273.3	−3.6	1.5	1.6
Arnarfell	64°13′02.3″	021°04′12.1″	MID-2	16.8	−21	18.1	−22.2	34.8	−21.6	11.1	–
Kálfstindar	64°13′06.2″	020°53′08.9″	MID-3**	48.8	−11.6	105.2	−7.9	154	−9.1	1.4	1.5
Nesjavellir	64°06′01.1″	021°14′50.4″	NES-1	32.8	−13.5	32.3	−3.3	65.1	−8.4	5.4	–
Ölfusvatnsfjöll	64°06′57.0″	021°08′26.4″	OLF-1	24.4	−11.2	13.5	−8.7	37.8	−10.3	2.4	2.9
Þrengsli	64°00′04.8″	021°27′45.4″	THREN-1**	23.4	−17.2	8.1	−13.4	31.5	−16.2	12.8	15.1
Reykjanesviti	63°48′44.6″	022°42′49.2″	REY-1**	50.7	−18.2	19.4	−20.8	70.1	−18.9	2.1	–
Hraunsvík	63°51′06.9″	022°22′07.2″	HRA-1**	16.2	−22	13.6	−14.2	29.9	−18.4	15.3	–
Mælifell	64°06′42.4″	021°10′51.5″	MAE-1**	17.9	−15.2	13.3	−7.5	31.2	−11.9	1.3	1.5
Lönguhlíðar	63°58′18.2″	021°56′42.2″	LON-1	17.5	−9.1	40	−7.8	57.4	−8.2	16.6	–
Ármannsfell	64°19′13.5″	020°59′43.9″	A1	23.4	−10	20.9	−8.6	44.3	−9.3	3.3	6.0
Þórólfsfell	64°26′55.6″	020°31′02.1″	A2	21.3	−16.3	22.3	−8.5	43.6	−12.3	3.6	4.2
Bláfell	64°30′56.3″	019°53′16.2″	A6	59.6	−26.7	98.1	−27.5	157.6	−27.2	28.0	29.9
Þverbrekknamúli-2	64°43′23.6″	019°36′52.7″	A8	13.4	−12.5	31	−9.1	44.4	−10.1	15.2	–
Arnarbæli	65°00′50.9″	019°35′20.7″	A9	14.6	−9.6	42.1	−6.9	56.7	−7.6	0.3	0.4
Eastern Rift Zone (ERZ)											
Skerðingar-1	64°34′17.8″	018°04′14.3″	A13/ICE08R-09	16.7	−11.9	27.8	−7.5	44.5	−9.2	5.5	6.5
Kambsfell	64°49′38.5″	017°45′19.8″	A20/ICE08R-15	30.9	−13.3	48	−6.6	78.8	−9.3	0.9	1.0
Gnjótsá near Kambsfell	64°49′36.7″	017°42′08.2″	A21/ICE08R-16	7.2	−16.1	27.8	−8.4	35	−10	0.1	0.2
North of Valafell	64°43′49.9″	017°42′30.7″	A22/ICE08R-17	34.9	−6.7	64	−7.1	99	−7	0.6	1.0
Mið-Bálkafell	64°40′22.8″	017°45′58.0″	A24	58.1	−25.1	52.4	−19.2	110.5	−22.3	14.5	19.1
Kirkjuellsvatn	63°58′44.5″	018°53′46.6″	A27	28.2	−6.5	20.1	−11.8	48.4	−8.7	4.5	8.7
NW of Grænifjallgarður	64°06′20.8″	018°30′55.5″	A32	31.4	−19.3	16.5	−16	47.9	−18.2	4.8	8.7
Sigalda	64°10′19.8″	019°08′18.7″	A35	10	−17	53.3	−7.9	63.3	−9.4	0.9	2.1
Heljargjá	64°19′19.8″	018°27′37.8″	A36/ICE08R-23	11.6	−17.2	7.5	−12.3	19.1	−15.3	35.4	–
Bláfjall	64°23′22.4″	018°13′45.2″	ICE08R-13	26.6	−20.4	23.3	−8.5	50	−14.8	1.0	1.0
Northern Rift Zone (NRZ)											
Hvammsfjöll	65°21′38.7″	016°41′11.4″	NAL-216	210.5	−7.2	34.8	−9.6	245.3	−7.6	10.3	17.8
Herðubreiðarfjöll	65°22′10.7″	016°22′29.5″	NAL-281	55.2	−16	44	−13.3	99.1	−14.8	1.5	–
Gæsahnjúkar	64°46′50.2″	017°30′40.7″	NAL-500	82.7	−12.5	43.6	−11.4	126.3	−12.1	8.3	–
Dyngjufjöll	65°09′42.1″	016°55′27.5″	NAL-584	49.5	−17.3	31.8	−26.4	81.2	−20.9	17.2	25.3
Upptyppingar	65°01′40.7″	016°13′44.4″	NAL-585	16.3	−17.1	20.4	−16.8	36.7	−16.9	11.6	14.2
Kistufell	64°47′23.8″	017°10′56.3″	NAL-595	54.4	−14.6	42.4	−12.3	96.9	−13.6	1.4	1.9
Kistufell	64°47′54.4″	017°12′01.2″	NAL-611	50.2	−6.9	15.2	−11.0	65.4	−7.9	0.8	–
Bláfjall	65°25′35.9″	016°48′56.2″	HS92-15	48.9	−8	67.3	−6.5	116.2	−7.1	1.0	1.2
Kvíhólafjöll	65°50′24.6″	016°59′10.4″	KVIH-1**	7	−14.1	24.3	−10.2	31.3	−11.1	20.7	51.4
Kvíhólafjöll	65°50′24.6″	016°59′10.4″	NAL-837**	8	−10	26.7	−5.6	34.6	−6.6	11.8	18.0
Hrúthálsar	65°19′25.7″	016°30′10.0″	NAL-828	13.4	−13.9	30.3	−5.1	43.7	−7.8	1.0	1.2
Kverkfjöll	64°49′00.0″	016°29′00.0″	KVK77	41.5	−25	41.9	−26.4	83.3	−25.7	40.4	–
Gæsahnjúkar	64°46′	017°29′	NAL-496**	79.3	−26.4	69.7	−24.9	149	−25.7	655	784
Eggert	65°15′	016°29′	NAL-688	15.2	−9.4	15.3	−10	30.5	−9.7	4.9	5.0
Upptyppingar	65°02′	016°14′	NAL-355**	23.5	−19.9	12.3	−13.3	35.8	−17.6	31.3	31.7
Upptyppingar	65°02′	016°14′	NAL-356**	25.1	−18.6	17	−16	42.1	−17.6	18.5	–
South Iceland. Volcanic Zone (SIVZ)											
Réttarfell (Þórsmörk)	63°40′19.5″	019°29′32.4″	RET-1	44.5	−8.5	13.7	−10.3	58.2	−8.9	9.4	–
Þríhyrningur	63°47′33.0	019°55′27.3	TRÍ-3	18.04	−16.5	22.9	−17.0	40.9	−16.8	1.3	–
Hekla Area	64°02′15	019°46′14	BHE-43	40.56	−18.6	26	−22.0	66.6	−20	2.2	–
Snæfellsnes Volcanic Zone (SNVZ)											
Ólafsvíkurenni	64°53′39	023°47′48	OLAF-1	11.6	−11.3	5	−12.7	16.5	−11.7	1330	–

Samples denoted with a double asterisk (**) are characterized by a late release of CO_2 during extraction and thus vesicle CO_2 = 700–1000 °C temperature steps and dissolved CO_2 = 1100–1200 °C temperature steps.

[a] 700–900 °C temperature steps.

[b] 1000–1200 °C temperature steps.

[c] 700–1200 °C temperature steps.

[d] Degassing-solubility corrected using $^4He/^{40}Ar^*$ ratio (See Section 5.3).

[*] All glasses belong to the tholeiitic series with the exception of SIVZ samples RET-1, TRÍ-3 and BHE-43, which belong to the transitional alkalic series and SNVZ sample OLAF-1, which belongs to the alkalic series (classification scheme after Jakobsson et al., 2008).

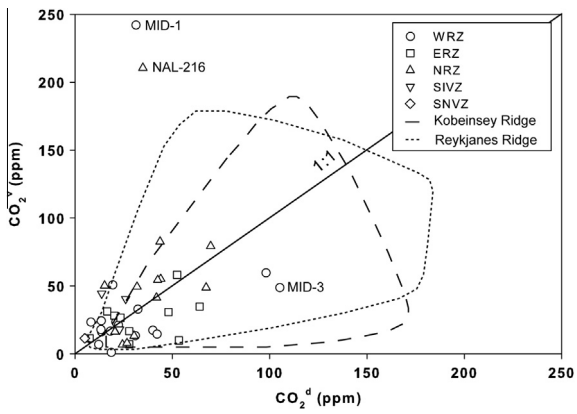

Fig. 5. Plot of CO_2 contained in vesicles (CO_2^v) vs. CO_2 dissolved in glass matrix (CO_2^d) measured by stepped heating methods. Magmatic CO_2 (CO_2^m) is uniformly divided between CO_2^v and CO_2^d in Iceland. Also shown are CO_2^v vs. CO_2^d values for the adjacent ridge segments: the Kolbeinsey (Macpherson et al., 2005a) and Reykjanes (de Leeuw, 2007) ridges.

empirically-derived FED trajectories have a slope between ~3.9‰ and 4.3‰ results in ~12–13% uncertainties on all C_p estimates.

In addition, we identify three samples (MID-2, REY-1, A6; circled in Fig. 6A) that fall well below the FED trajectory and therefore cannot be explained by degassing fractionation alone. Notably, all three samples display $\delta^{13}C$ values lower than −20‰ and have higher than expected CO_2 contents considering their extreme $\delta^{13}C$ values. Similar observations are made for the NRZ and ERZ samples (circled values – Fig. 6B and C) and indicate possible assimilation processes involving an isotopically-low $\delta^{13}C$ component (see Section 5.2.3). In contrast to these low $\delta^{13}C$ samples, one sample (NES-1) stands alone with high $\delta^{13}C$ – plotting above the BED line (Fig. 6A). As a result, C_p cannot be determined analytically for this particular sample, but can be approximated using a graphical approach, whereby the BED trajectory is assumed, and then forced to pass through point NES-1. However, if we assume that degassing is sufficiently advanced (>80%) so that the change in $\delta^{13}C$ from the initial value is approximately equal to Δ (+4.3‰) then NES-1 (−3.3‰) would require a positive mantle starting carbon isotope composition, which is highly unlikely in the context of anticipated mantle values and other values in this study. Alternatively, high $\delta^{13}C$ values can result from crustal assimilation of a ^{13}C enriched end-member (i.e., carbonates) in the magma chamber or magma conduits. Notably, most basalts in this study that fall outside of the mixing envelope defined by BED and FED trajectories are affected by addition of carbon with lower (organic/sedimentary) $\delta^{13}C$ values.

Estimating pre-eruptive CO_2 source compositions from the two remaining neovolcanic rift zones is more complicated due to the lack of a clearly defined BED trajectory, in the case of the NRZ (Fig. 6B), and a FED trajectory in the case of the ERZ (Fig. 6C). As a result, C_p cannot be determined analytically as described above for the WRZ so must be approximated using a graphical approach. In the NRZ, the FED trend can be defined by the slope of a best fit regression through samples NAL-356, NAL-281, NAL-500 and NAL-595, resulting in a slope of (Δ=) ~3.9‰. However, no clear BED trend exists and therefore we estimate starting values by forcing the BED trajectory through just one sample – NAL-828 ($C_{rBED} = 30.3$ ppm, $\delta_r = -5.1$‰). Again, if our assumptions hold true and degassing is sufficiently advanced (>80%), as with the majority of Iceland basalts, the change in $\delta^{13}C$ from the initial value is ~3‰ and therefore NRZ samples would require starting compositions of $C_p = 550 \pm 66$ ppm and $\delta_p = -2.0 \pm 1.0$‰, respectively (Fig. 6B). As in the WRZ, three samples plot well below the FED trajectory and require crustal assimilation to explain their extreme values.

In the ERZ, there is no clearly defined FED trajectory, so we use an average Δ-value (from WRZ and NRZ) of +4.1‰. We then select ERZ samples A22 ($C_rBED^1 = 64.0$ ppm, $\delta_r^1 = -7.1$‰) and A13 ($C_rBED^2 = 27.8$ ppm, $\delta_r^2 = -7.5$‰), which follow a BED trajectory and calculate C_rFED^1 and C_rFED^2. With C_rBED^1 and C_rFED^1 and C_rBED^2 and C_rFED^2, we estimate C_p using Eq. (5) and δ_pBED^1, δ_pBED^2, δ_pFED^1, and δ_pFED^2 using Eqs. (2) and (3), respectively. The estimated CO_2 composition of pre-eruptive melt is $(C_p) = 371 \pm 45$ ppm, with a corresponding average $\delta_p = -3.7 \pm 1.0$‰ (Fig. 6C). Notably, one ERZ sample (A24) falls well below the FED trajectory. We also note that source estimates for NRZ and ERZ samples are obtained using a graphical approach, and are therefore highly model and assumption dependent.

By combining carbon data ($n = 47$) from all three neovolcanic rift zones as well as from the SNVZ and SIVZ, we can estimate pre-eruptive CO_2 source estimates for Iceland as a whole (Fig. 6D). Seven samples were selected to define the FED trajectory: SKARD-1 and MID-3 from the WRZ, NAL-356, NAL-281, NAL-500 and NAL-595 from the NRZ and A32 from the ERZ. A fractionation factor of (Δ=) ~4.2‰ was determined by calculating the slope of a best-fit regression line ($\delta_r = 4.19\ \ln(C_rFED) - 27.87$) (see Fig. 6D) through these ($n = 8$) samples. We then selected ERZ sample A-22 ($C_rBED^1 = 64.0$ ppm, $\delta_r^1 = -7.1$‰) and WRZ sample MAE-1 ($C_rBED^2 = 13.3$ ppm, $\delta_r^2 = -7.5$‰), which follow a BED trajectory and calculate C_rFED^1 and C_rFED^2 using the FED regression line. The resultant estimated CO_2 composition of the pre-eruptive melt taking all of the neovolcanic zone samples together is $(C_p) = 531 \pm 64$ ppm, with a corresponding average $\delta_p = -2.5 \pm 1.1$‰ (i.e., average of δ_pBED^1, δ_pBED^2, δ_pFED^1, and δ_pFED^2) (Table 3).

Pre-eruptive carbon estimates of Icelandic basalts reveal several interesting features: (1) CO_2 source estimates increase from the WRZ (206 ± 24 ppm) to the ERZ (371 ± 45 ppm) and reach a maximum in the NRZ (550 ± 66 ppm), (2) average source estimates ($C_p = 531 \pm 64$ ppm) are in good agreement with previous estimates for DMM primary melts of 367–858 ppm CO_2 assuming 12% partial melting (Marty, 2012) and, olivine-hosted melt inclusions (430–510 ppm CO_2) from the Laki eruption (Metrich et al., 1991), and overlap with estimates of ~400 ± 100 ppm from the adjacent Reykjanes and Kolbeinsey ridges, (3) the δ_p (=−2.5 ± 1.1‰) estimate using all

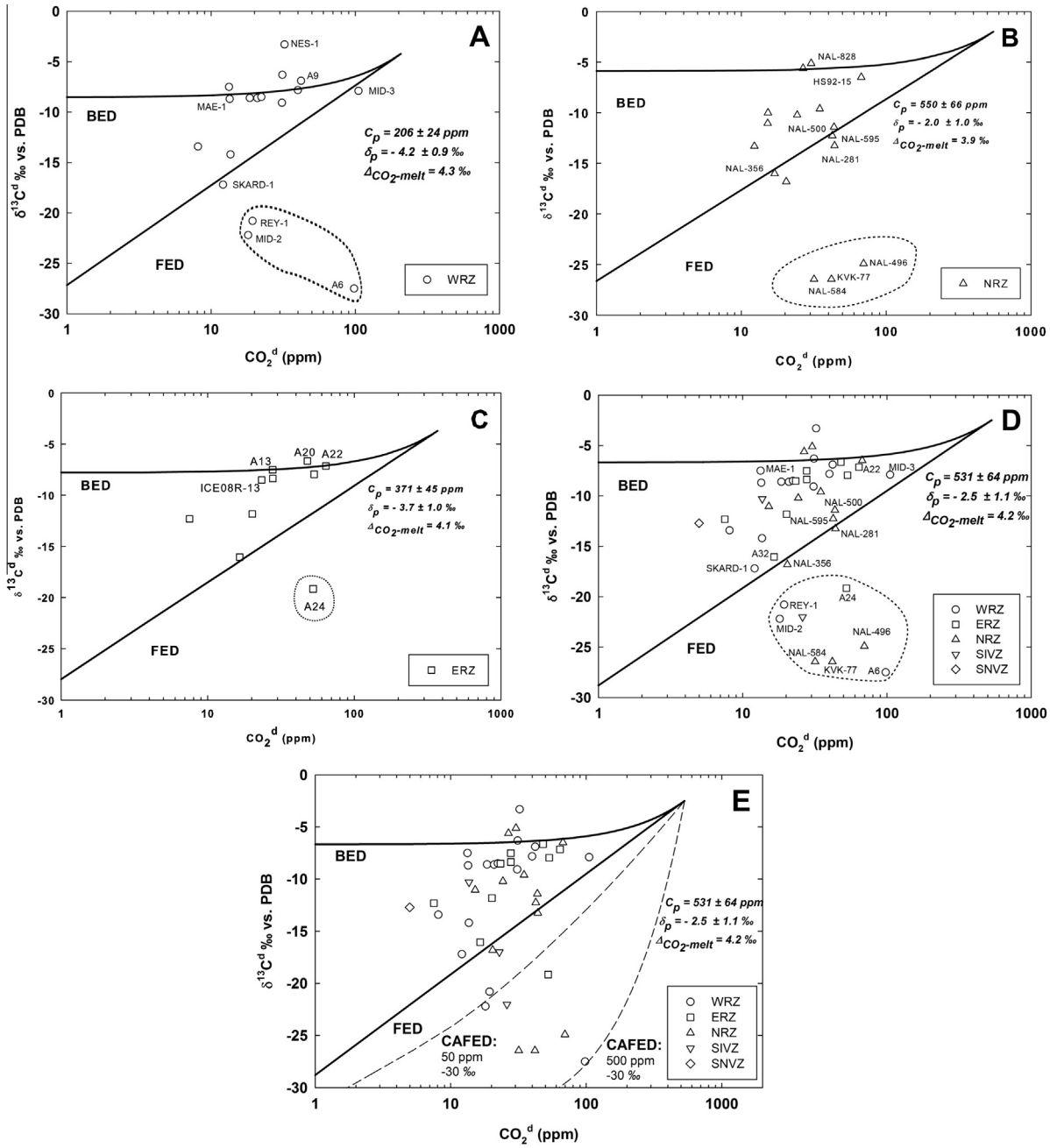

Fig. 6. (A–E) Carbon-isotopes ($\delta^{13}C$) as a function of dissolved CO_2 content (ppm) in basalts of the various volcanic zones of Iceland: (A) WRZ; (B) NRZ; (C) ERZ; (D and E) All Iceland data. *Solid lines:* calculated BED and FED mixing trajectories. *Circled dashed lines:* samples effected by CAFED. Panel E considers assimilation of isotopically light carbon in concert with FED. *Dashed lines:* calculated CAFED mixing trajectories.

of the neovolcanic zone samples together is similar to the average geothermal value of $-3.1 \pm 1.9‰$ reported in section 4.1.1 – suggesting that geothermal fluid carbon isotope signal closely resembles the primary mantle composition of Iceland obtained using the basalt approach. We note that this is not a unique solution and that subglacial basalt carbon data could also be explained using a Δ value = 2.3‰ (lowest experimentally-derived value; Mattey, 1991) and pre-eruptive melt compositions of ~400 ppm and −3‰. However, if a Δ-value of 2.3‰ is adopted then a significantly larger (>50%) fraction of the data would require crustal addition (CAFED mixing – see Section 5.2.3) to explain their carbon systematics. We note also that pre-eruptive CO_2 estimates of ~531 ppm are lower than some estimates for primitive MORB (Cartigny et al., 2001; Saal et al., 2002) and plume-derived settings (Aubaud et al., 2005, 2006), suggesting that the Iceland mantle source may be relatively carbon poor. Alternatively, degassing

Table 3
Calculations of CO_2 in pre-eruptive melts.

	C_rBED[1] (MAE-1)	C_rBED[2] (A-22)	C_P	δ_P
δ_r (‰)	−7.5	−7.1	531[c]	−3.4[d]
C_rBED (ppm)	13.3	64.0		−3.4[e]
C_rFED (ppm)	128.9[a]	141.8[b]		−1.6[f]
				−1.6[g]

[a] Calculated from δ_r^1 and the regression line (FED trajectory).
[b] Calculated from δ_r^2 and the regression line (FED trajectory).
[c] Calculated from Eq. (5).
[d] Calculated from Eq. (2) using δ_r^1 and C_rBED[1].
[e] Calculated from Eq. (2) using δ_r^2 and C_rBED[2].
[f] Calculated from Eq. (3) using δ_r^1 and C_rFED[1].
[g] Calculated from Eq. (3) using δ_r^2 and C_rFED[2].

may have occurred prior to equilibration beneath Iceland and as a result, pre-eruptive CO_2 estimates should be regarded as minimum values.

5.2.3. Coupled assimilation and fractional equilibrium degassing (CAFED)

Fig. 6A–D demonstrate that most (>80%) samples can be bracketed between BED and FED degassing trajectories and, as a result, the majority of Iceland CO_2 data can be adequately described by the above two-stage degassing model. However, several ($n = 8$) clear outliers plot below the well-defined FED trajectory and are marked by substantially lower $\delta^{13}C$ values compared to samples with similar CO_2 contents (circled values Fig. 6D). While it is possible that the low $\delta^{13}C$ represents post-eruptive contamination on glass surfaces, every precaution was taken in cleaning these glasses prior to stepped-heating analysis (Section 3.2). Notably, the low $\delta^{13}C$ contaminant is observed in the dissolved phase (i.e., 900–1200 °C heating step) and, therefore, this possibility is unlikely. Alternatively, these glasses may be derived from magma with a distinctively lower initial $\delta^{13}C$ value than the remainder of the Icelandic suite. However, no other geochemical features of these samples suggests that they were derived from a source different from other Icelandic basalts (Füri et al., 2010) and, furthermore, low $\delta^{13}C$ values are observed in all three axial rift zones. Therefore, the most likely explanation for these data is that they were derived from similar pre-eruptive magma as other Icelandic samples but acquired low $\delta^{13}C$ during interaction with the crust. Assimilation processes have been suggested for the adjacent Kolbeinsey Ridge (Macpherson et al., 2005a). Notably, the relatively rare occurrence of extremely low $\delta^{13}C$ suggests that most magma batches avoided interaction with low $\delta^{13}C$ (organic/sedimentary-derived) crust. Alternatively, the carbon isotopic composition of the wall rock may have been predominantly magma-like, and thus modification to the $\delta^{13}C$ of the magma was negligible.

In order to investigate the concurrent processes of degassing and wall rock assimilation, we adopt the approach of Macpherson et al. (2010) and construct a coupled assimilation and fractional equilibrium degassing (CAFED) model in which FED occurs in increments of 1%, followed by assimilation with contaminant CO_2 between 50 and 500 ppm and $\delta^{13}C = -30‰$. FED was selected due to the longer storage and eruption times associated with open system degassing which should promote interaction between melts and contaminants. This model assumes that the thick Icelandic crust is heterogeneous and likely stratified with respect to carbon speciation and isotope signatures. Average CO_2 contents of ~500 ppm, measured in altered basalts from IRPD drill cores in eastern Iceland (Flower et al., 1982) and in oceanic drill cores (Shilobreeva et al., 2011), are used as a potential CAFED crustal endmember in the model. We postulate that low $\delta^{13}C$ organic signatures in crustal wall rocks result from either hydrothermal circulation of organic material (Lang et al., 2006) and/or biological activity during mineralization (Thorseth et al., 1992; Fisk et al., 2003). Carbonates associated with microbially-altered volcanic glasses have shown large $\delta^{13}C$ variations, ranging from −16‰ up to +5‰ (Furnes et al., 2001) and $\delta^{13}C$ values of total organic carbon (TOC) from serpentinized peridotites and gabbroic rocks from the Lost City Hydrothermal System range from −28.9‰ to −21.5‰ (Delacour et al., 2008). Alternatively, this depleted component might represent highly degassed material (lavas) that comprise the bulk of the Icelandic crust. Fig. 6E plots $\delta^{13}C^d$ vs. CO_2^d for all Icelandic subglacial basalt data and illustrates that samples ($n = 8$) with extremely low $\delta^{13}C$, which fall below the FED trajectory, can be explained by CAFED (dashed lines) with the contaminant marked by $CO_2 = 50$–500 ppm and $\delta^{13}C = -30‰$. This figure illustrates that by adopting a CAFED-type model, which incorporates crustal interaction with the melt, we can effectively generate extremely low $\delta^{13}C$ values at relatively high CO_2^d contents that cannot otherwise be resolved by traditional fractional equilibrium models.

5.2.4. Vesicle CO_2 and noble gas elemental fractionation

In addition to the new CO_2 concentration and isotope data presented here, a subset ($n = 30$) of Icelandic glasses were previously characterized for vesicle-sited He, Ne, and Ar concentrations and isotopes (Füri et al., 2010). By combining these two data sets, we calculate volatile ratios (i.e., $CO_2/^3He$ and CO_2/Ar^*), which, when combined with previously reported $^4He/^{40}Ar^*$ ratios (Füri et al., 2010), reveal important additional information about the degassing histories of the magmas.

The extent of degassing can be gauged by the $^4He/^{40}Ar^*$ ratio (Marty and Tolstikhin, 1998), assuming a $^4He/^{40}Ar^*$ mantle production ratio of ~2 (Jambon et al., 1986). Füri et al. (2010) showed that low $^3He/^4He$ ratios are not coupled with low helium concentrations, suggesting that crustal contamination has a negligible effect on He-isotopes (Hilton et al., 1993, 1995; Macpherson et al., 1998, 2005a; Füri et al., 2010) so that $^4He/^{40}Ar^*$ should reflect the effects of degassing only. Furthermore, $^4He/^{40}Ar^*$ values plot near, or above the mantle production ratio in nearly all Icelandic basalts, due to preferential loss of Ar during degassing (Füri et al., 2010).

Having identified samples that have been modified by both degassing and crustal assimilation processes (Section 5.2.3), we now plot (Fig. 7A–C) elemental ratios of vesicle-sited volatiles in order to highlight elemental fractionation that occurs during vesicle formation due to

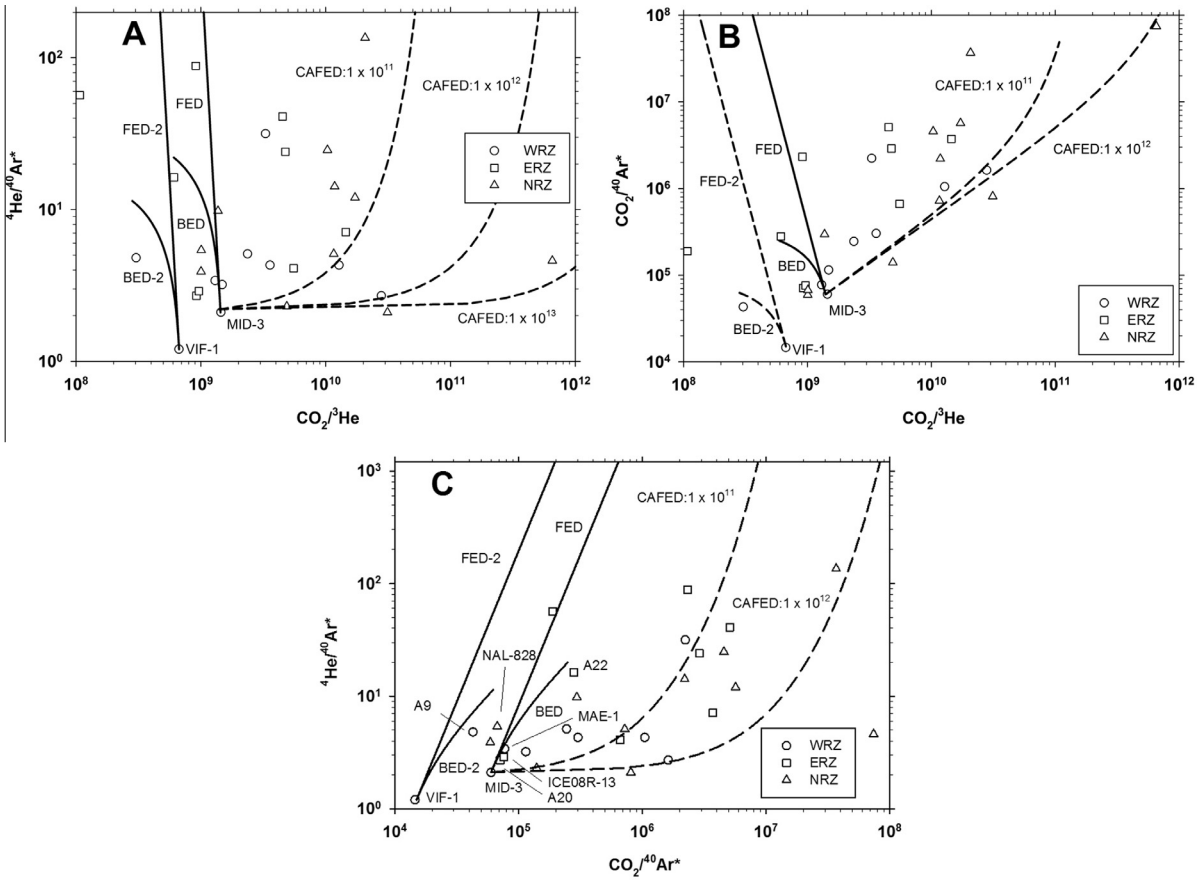

Fig. 7. (A–C) Elemental ratios for vesicle derived gases from Iceland's neovolcanic axial rift zones. (A) $CO_2/^3He$ vs. $^4He/^{40}Ar^*$; (B) CO_2/Ar^* vs. $CO_2/^3He$; (C) $^4He/^{40}Ar^*$ vs. CO_2/Ar^*. Superimposed on each subplot are two equilibrium degassing scenarios (FED-BED & FED-2-BED-2; solid lines) and coupled assimilation fractional equilibrium degassing (CAFED) scenarios. Starting compositions: MID-3 ($^4He/^{40}Ar^* = 2.1$; $CO_2/^{40}Ar = 6.0 \times 10^4$; $CO_2/^3He = 1.4 \times 10^9$) and VIF-1 ($^4He/^{40}Ar^* = 1.2$, $CO_2/^{40}Ar^* = 1.5 \times 10^4$, $CO_2/^3He = 6.7 \times 10^8$) correspond to FED-BED and FED-2 and BED-2 and CAFED processes, respectively. The CAFED assumes 1% degassing increments from a given starting composition, followed by addition of contaminant. $CO_2/^3He$ and CO_2/Ar^* values of the crustal contaminant are assumed to be enriched by a factor of $\sim 10^2$–10^4, which is consistent with their crustal provenance (e.g., $CO_2/^3He = 1 \times 10^{11}$–$1 \times 10^{13} = CO_2/^3He$ of contaminant; O'Nions and Oxburgh, 1988). Following assimilation, the degassing step is repeated from the new starting composition. Various samples (MID-3, A-9, MAE-1, NAL-828, A20, ICE08R-13 and A22), which are used to define BED trajectories in Fig. 6, have been labelled in order to demonstrate that degassing is affecting carbon and other volatiles similarly, however samples SKARD-1, NAL-281, NAL-356 and NAL-500 are not plotted due to the fact that $^4He/^{40}Ar^*$ values were not determined for these samples.

relative solubility differences between species (i.e., $S_{He} = 6.4 \times 10^{-4}$ cm^3 STP/g, $S_{CO_2} = 2.7 \times 10^{-4}$ cm^3 STP/g, and $S_{Ar} = 6.8 \times 10^{-5}$ cm^3 STP/g at 1 bar atm; Jambon et al., 1986; Lux, 1987; Pan et al., 1991; Dixon and Stolper, 1995; Jendrzejewski et al., 1997; Hilton et al., 1998a; Cartigny et al., 2001). We begin by assuming that WRZ sample MID-3 ($^4He/^{40}Ar^* = 2.1$; $CO_2/^{40}Ar = 6.0 \times 10^4$; $CO_2/^3He = 1.4 \times 10^9$) can be used to approximate the least degassed sample, and thus provides a useful starting point to consider degassing and coupled assimilation in Icelandic basalts. This assumption is consistent with the dissolved carbon isotope and abundance systematics of MID-3 (Section 5.2.3), which indicates that this sample has undergone little modification. Füri et al. (2010) also used nearby sample (MID-1) from the adjacent Miðfell region to approximate the undegassed mantle source using He–Ne–Ar isotope characteristics. Both BED and FED trajectories are then plotted using this presumed starting composition. Notably, labelled samples (e.g., MID-3, A-9, MAE-1, NAL-828, A20, ICE08R-13 and A22) that fall along BED trajectories in Fig. 7C correspond to samples used to empirically define BED trajectories in Section 5.2.2 (e.g., Fig. 6). Likewise, samples that display extremely low $\delta^{13}C$ values in Fig. 6 also require CAFED mixing to explain their extreme values. Relative solubility differences between elements leads to increases in $^4He/^{40}Ar^*$and $CO_2/^{40}Ar^*$ and a decrease in $CO_2/^3He$ in the residual phase as degassing progresses. However, in some instances the two models do not agree; for example, Fig. 6A suggests that A9 and MID-3 result from degassing of the same magma, yet their $^4He/^{40}Ar^*$–$CO_2/^{40}Ar^*$ compositions cannot be related by any simple degassing scenario. As seen in all three sub-plots of Fig. 7, BED and FED degassing trajectories provide a reasonable fit to a small proportion of samples and thus

an additional process must be considered. For example, several samples with distinctly high $CO_2/^3He$ values are accompanied by relatively low $^4He/^{40}Ar^*$ values (Fig. 7A). Such high $CO_2/^3He$ values cannot be produced by degassing alone: this process would require unrealistically high starting $CO_2/^3He$ values or volatile solubilities that are drastically different than experimentally-derived values. Alternatively, assimilation of crustal material ($CO_2/^3He = 1 \times 10^{11}$–$1 \times 10^{13}$, $^4He/^{40}Ar^* = 2$) could provide a mechanism to produce the observed variations. Such a process would be consistent with assimilation of ^{13}C-depleted wall rock into the melt during transfer to the surface, and would likely occur concurrently with degassing. Thus, the approach of Macpherson et al. (2010) can be used to construct a CAFED type model to illustrate this process.

The majority of samples plot close to CAFED trajectories, allowing us to conclude that CAFED is necessary to explain the majority of Iceland samples. In this case, wall rock assimilation is an important control on the volatile systematics of Iceland. However, this approach does not account for several low (vesicle) $CO_2/^3He$ samples which cannot result from degassing (assuming MID-3) and/or through CAFED. Therefore, we suggest heterogeneities in elemental source characteristics as a potential explanation. Alternatively, Hahm et al. (2012) suggested that selective assimilation of pure CO_2 by the largest vesicles in the magma could provide the mechanism to produce lower $CO_2/^3He$ (and $CO_2/^{40}Ar^*$) values with minimal modification to $^4He/^{40}Ar$ ratios.

In summary, the relative abundance characteristics of vesicle-sited CO_2 and other volatiles are compatible with degassing and assimilation of crustal material (in most cases). We postulate that parent magma is stored in crustal magma chambers where addition of CO_2 can occur, most likely due to wall rock interaction.

5.3. CO_2 flux estimates

Having identified intrinsic CO_2 characteristics of Icelandic fluids/gases (Section 5.1) and subglacial basalts (Section 5.2), we are now able to estimate the total CO_2 output from Icelandic magmatic systems. CO_2 fluxes are estimated using three different approaches: (1) combining ^3He flux estimates from Iceland (Hilton et al., 1990, 1998b) with measured $CO_2/^3He$ values (this study); (2) estimating pre-eruptive CO_2 contents of basaltic melts (this study) and combining these data with magma production rates for Iceland (Schilling et al., 1978, Crisp, 1984; White, 1993; Armannsson et al., 2005), and (3) by combining geothermal fluid flow rates (Gıslason et al., 1992; Agustsdottir and Brantley, 1994; Gıslason, 2000; Kristjansson et al., 2004; Armannsson et al., 2005; Fridriksson et al., 2006) with measured CO_2 contents in fluids (this study). These estimates are then compared to previous estimates of the CO_2 output from Iceland, determined by integrating steam flow rates with CO_2 concentrations in HT steam fields (Armannsson et al., 2005; Fridriksson et al., 2006) and fluid flow rates at individual volcanic centers (Gıslason, 1992, 2000; Agustsdottir and Brantley, 1994). All CO_2 flux estimates for Iceland are tabulated and compared to other volcanic/geothermal areas worldwide and global rift zones in Table 4.

The ^3He flux at mid ocean ridges (MOR) was first reported by Craig et al. (1975), who measured relative ^3He enrichments in seawater around MOR-crests and estimated a primordial ^3He flux ($\sim$1000 mol a^{-1}) from the Earth's mantle. By combining ^3He flux estimates with measured $CO_2/^3He$ values from individual rift segments, CO_2 fluxes have been quantified in various global rift segments such as the East Pacific Rise and the Mid-Atlantic Ridge (Marty and Jambon, 1987; Marty and Tolstikhin, 1998). However, more recent estimates (Farley et al., 1995; Saal et al., 2002; Bianchi et al., 2010) suggest that ^3He fluxes may be overestimated by a factor of $\sim$2 and, as a result, previous global ridge CO_2 flux estimates (Marty and Tolstikhin, 1998) would represent upper limits. In this contribution, we report $CO_2/^3He$ values from both geothermal manifestations and subglacial basalts of Iceland, both of which can be combined with ^3He fluxes from Iceland to estimate CO_2 fluxes. We then compare these results with other plume-related regions worldwide as well as other subaerial volcanic regions.

In Section 5.1, we showed that $CO_2/^3He$ values measured in fluids and off-axis gas samples were extensively modified and therefore only on-axis free gas phase samples (mean $CO_2/^3He = 5.9 \pm 6.3 \times 10^9$; $n = 37$) can be considered appropriate for estimating CO_2 fluxes. In contrast, all on-axis basalt ($n = 43$) $CO_2/^3He$ values (mean $CO_2/^3He = 24 \pm 99 \times 10^9$) are considered appropriate to approximate source values: however, some of the $CO_2/^3He$ variability must be due to degassing and/or CAFED (Section 5.2), and thus a similar filter must be applied to the data. In order to circumvent the effects of degassing on basalt samples, a simple degassing correction (after Marty and Tolstikhin, 1998) can be applied to raw data by assuming that Ar loss follows a Rayleigh distillation (Marty, 1995). While our modelling results suggest that degassing is likely a combination of both open and closed system degassing, we suggest, based on extreme C-isotopes and $^4He/^{40}Ar$ values, that open system degassing is the dominant process. In this way, any degassing fractionation effect between two volatiles can be scaled to the $^4He/^{40}Ar^*$ ratio. Using this approach, we calculate initial $CO_2/^3He$ ratios according to:

$$(CO_2/^3He)_{initial} = (CO_2/^3He)_{obs} \times \left[(^4He/^{40}Ar^*)_{obs}/(^4He/^{40}Ar^*)_{initial}\right] \wedge \left[1 - (S_{He}/S_{CO2})/1 - (S_{He}/S_{Ar})\right] \quad (6)$$

As degassing progresses, residual $^4He/^{40}Ar^*$ values increase and $CO_2/^3He$ values decrease (Marty and Tolstikhin, 1998; Hilton et al., 1998a). Consequently, the average measured $CO_2/^3He$ value of Icelandic basalts of $24 \pm 99 \times 10^9$ can be corrected to a mean starting value of $\sim 35 \pm 140 \times 10^9$. Importantly, by using extreme carbon isotope values as a metric for extent of crustal modification (Fig. 6E; circled samples), we can identify and selectively remove ($n = 7$)

Table 4
CO_2 flux estimates.

Study area	CO_2 flux (mol/year)$\times 10^{10}$	% of global ridge flux	Method	References
Iceland	7–23[b]	3–10[b]	He flux and $CO_2/^3He$	This work[a]
Iceland	0.2–0.8[b]	0.1–0.4[b]	Primary melt $CO_2 = 531$ ppm CO_2	This work[a]
Iceland	7	3	TDIC and flow rate extrapolated	Gislason (1992, 2000) and Agustsdottir and Brantley (1994)
Iceland	2–5	1–2	Heat flux and Steam vent and diffuse soil emissions	Arnórsson (1991), Arnórsson and Gıslason (1994), Kristjansson et al. (2004) and Fridriksson et al. (2006)
Global Ridge	220	–	He flux and $CO_2/^3He$	Marty and Tolstikhin (1998)
Plume-related Regions				
Kilauea, Hawaii	0.1–3.0	0.1–1	Primary melt estimates	Greenland et al. (1985), Gerlach and Graeber (1985), Dixon and Clague (2001), Hauri (2002) and Crisp (1984)
Reunion	0.1–0.2	0.1	Primary melt estimates	Bureau et al. (1998)
Society Islands	0.2	0.1	Primary melt estimates	Aubaud et al. (2005)
Pitcairn	0.2	0.1	Primary melt estimates	Aubaud et al. (2006)
Yellowstone	23–50	10–23	Basalts and hydrothermal	Werner and Brantley (2003)
Subaerial Volcanic Regions				
Solfatara, Italy	0.1	0.1	Diffuse soil emissions	Chiodini et al. (1998)
Etna, Sicily	100	45	CO_2/SO_2 ratio	Allard et al. (1991)
Central American Arc	6–7	3	He flux and $CO_2/^3He$	Hilton (2002) and Shaw et al. (2004)
Oldoinyo Lengai, Tanzania	0.06	–	IR and diffuse soil emissions	Brantley and Koepenick (1995)
Mt. Erebus, Antarctica	1.5	0.7	CO_2/SO_2 ratio	Wardell and Kyle (1998)
White Island, NZ	2.2	1	CO_2/SO_2 ratio	Wardell and Kyle (1998)
Aggregate Fluxes				
Subaerial (Arc + Plume)	148–550	–	–	Varekamp et al. (1992), Williams et al. (1992), Marty and Tolstikhin (1998)
Global Ridge (MOR)	68–2300	–	–	Varekamp et al. (1992), Morner and Etiope (2002), Kerrick (2001), Marty and Tolstikhin (1998)
Global Total	295–2300	–	–	Gerlach (1991), Le Cloarec and Marty (1991), Varekamp et al. (1992), Sano and Williams (1996), Morner and Etiope (2002), Kerrick (2001), Delgado et al. (1998) and Marty and Tolstikhin (1998)

[a] ^3He flux of ~10–36 mol a^{-1}.
[b] Using crustal production rate of 0.064–0.22 km^3 a^{-1} (Hilton et al., 1990, 1998b; White, 1993; Armannsson et al., 2005).

samples that have been largely affected by crustal assimilation; we thus consider only the remaining on-axis samples to be representative of the source composition. Using this approach, an average $CO_2/^3He$ value of $7.9 \pm 12 \times 10^9$ can be calculated for the remaining basalts, which is in good agreement the average value $5.9 \pm 6.3 \times 10^9$ reported here for selected ($n = 37$) gas phase samples, as well as previous $CO_2/^3He$ estimates (6×10^9; Poreda et al., 1992) from HT fluids from the axial rift zones of Iceland. We caution that due to the large uncertainties associated with these estimates they can only be used to place an upper limit on the CO_2 flux.

Previously, Hilton et al. (1990, 1998b) derived a ^3He flux of ~11 mol a^{-1} from Iceland using a measured ^4He flux of 6×10^9 cm^3 STP ^4He a^{-1}, 10% partial melting, a crustal production rate of 0.064 km^3 a^{-1}, an estimated He concentration in the mantle source of $\sim 30 \times 10^{-5}$ cm^3 STP/g basalt, based on an assumed $^3He/^4He$ ratio for Iceland of 30 R_A. Average filtered gas and basalt $CO_2/^3He$ values can then be combined with this ^3He flux in order to estimate a CO_2 flux of ~ 7–9×10^{10} mol a^{-1}. Notably, the ^3He flux estimate of Hilton et al. (1998b) assumes a crustal production estimate of 0.064 km^3 a^{-1} (Schilling et al., 1978; Crisp, 1984; Hilton et al., 1990, 1998b); however, estimates of crustal production in Iceland vary widely. For example, if we assume basaltic magma is emplaced into the Icelandic crust along the ~550 km axial rift zone, with a spreading rate of 2 cm a^{-1} (Bjornsson, 1985) and an average crustal thickness of ~20 km (Bjarnason et al., 1993), then we calculate a crustal production rate of ~0.22 km^3 a^{-1}, which is in agreement with other estimates (White, 1993; Armannsson et al., 2005). By adopting higher crustal production rates, we estimate a significantly larger CO_2 flux of $\sim 23 \times 10^{10}$ mol a^{-1} for Iceland. This latter value represents ~10% of the global ridge flux (Marty and Tolstikhin, 1998). For

perspective, Iceland comprises just less than 1% of the length of the global ridge system. Together, these results suggest that higher crustal production rates in Iceland coupled with DMM-like CO_2 contents in the Icelandic mantle source can potentially result in proportionally large CO_2 fluxes relative to global ridge averages.

The second approach to estimating the mantle CO_2 flux involves combining pre-eruptive CO_2 source estimates for Iceland (400–531 ppm; Section 5.2) with magma production rates between 0.064 and 0.22 $km^3\ a^{-1}$ (Hilton et al., 1990; White, 1993; Armannsson et al., 2005), which are considered a reasonable approximation for olivine-tholeiites (i.e., the most common magma type generated in rift zones of Iceland; Slater et al., 1998; Momme et al., 2003; Marty, 2012). This approach assumes that carbon is highly incompatible (Bottinga and Javoy, 1990) and thus passes efficiently into the melt phase, and is quantitatively degassed from basaltic melt during magma ascent. This latter assumption is supported by empirical observations (Fig. 6E). Using this approach, we calculate a CO_2 flux between 0.2 and 0.8 ($\times 10^{10}$ mol a^{-1}), which represents 0.1–0.4% of the global ridge flux (Marty and Tolstikhin, 1998). Notably, these estimates overlap with previous estimates of other plume-related regions (Table 4). In addition, by combining CO_2 source estimates (Section 5.2.2) for the individual rift segments (WRZ = 206 ± 24 ppm; ERZ = 371 ± 45 ppm; NRZ = 550 ± 66 ppm) with crustal production rates (scaled to rift segment length; WRZ = ~210 km, ERZ = ~140 km, NRZ = ~200 km), we can estimate CO_2 output from individual rift zones. In this way, a range of values from 0.1 to 0.3×10^{10} mol a^{-1} are calculated for the WRZ, 0.11–0.22×10^{10} mol a^{-1} for the ERZ and 0.11–0.3×10^{10} mol a^{-1} for the NRZ (40%, 25% and 35% of the total, respectively).

Finally, measured geothermal fluid CO_2 contents (TDIC) can be combined with estimated regional fluid discharge rates (Heng, 2004) to make a first order estimate of CO_2 fluxes from Iceland via geothermal discharges. Notably, the ERZ is the only axial rift segment where fluid phase samples were collected and thus the only region where we are able to estimate CO_2 fluxes. In addition, several fluid samples were collected in LT off-axis portions of the crust (i.e., SISZ and Vestfirðir); however, these samples are substantially modified by calcite precipitation (Section 5.1.3) and, as a result, have almost certainly lost much of their primary CO_2, as is evident by their low CO_2 contents (typically < 1 mmolCO_2/kg H_2O). Using an average CO_2 content of ~2.84 mmolCO_2/kg H_2O measured at Köldukvíslabotnar (ERZ), and previously published fluid flow estimates of ~1000–2000 l/s (Heng, 2004) for the Köldukvíslabotnar region, we calculate a CO_2 flux of 0.9–1.8×10^8 mol a^{-1} for this segment of the ERZ. Unfortunately, published fluid flow estimates are not available for the remainder of the ERZ and thus CO_2 flux estimates cannot be directly determined for the individual localities. However, if we assume that fluid discharge rates are relatively constant throughout the ERZ, we can calculate CO_2 outputs between 0.6–1.2×10^8 mol a^{-1} for Landmannalaugar and 1.7–3.5×10^8 mol a^{-1} for the Vonarskarð region.

We compare our three estimates with previously published CO_2 flux estimates for Iceland – determined by integrating fluid and steam fluxes with measured CO_2 contents. In total, CO_2 flux estimates have been calculated for just 4 of ~40 volcanic and geothermal systems of Iceland (Armannsson et al., 2005): Hekla (Gıslason et al., 1992), Grímsvötn (Agustsdottir and Brantley, 1994), Eyjafjallajökull (Gıslason, 2000), and Reykjanes (Kristjansson et al., 2004; Fridriksson et al., 2006). At Grímsvötn and Eyjafjallajökull, [CO_2] was measured in subglacial calderas where magmatic CO_2 is dissolved in glacial melt-water. During subsequent catastrophic flooding events (i.e., jökulhlaups) flow-rates were measured and combined with [CO_2] in order to estimate CO_2 fluxes. Notably, Grímsvötn is one of the largest and the most active volcanic system in Iceland, and thus the CO_2 flux (~44×10^8 mol a^{-1}; Agustsdottir and Brantley, 1994) is approximately an order of magnitude larger than other less active regions, such as Eyjafjallajökull (0.6–6×10^8 mol a^{-1}; Gıslason, 2000). Notably, the later estimates from Eyjafjallajökull are valid during periods of volcanic dormancy. However, during 5 weeks of activity in April–May, 2011 the volcano emitted an estimated 1.3×10^{11} mol CO_2 (Allard et al., 2010), an amount comparable to total flux estimates for Iceland over one (dormant) year (i.e., 0.2–23×10^{10} mol a^{-1}). Using a similar approach, Gıslason et al. (1992) estimated CO_2 discharge into the local groundwater system from the Hekla magma chamber to be ~16×10^8 mol a^{-1}. In addition, Kristjansson et al. (2004) and later Fridriksson et al. (2006) reported a CO_2 flux through soils in the Reykjanes geothermal area to be ~6×10^8 mol a^{-1}. The combined CO_2 flux for these four volcanic centers is ~0.7×10^{10} mol a^{-1}: however, if this value is extrapolated to include the remaining ~35–40 geothermal/volcanic systems of Iceland, the resultant flux is ~7×10^{10} mol a^{-1} (Gıslason et al., 1992; Agustsdottir and Brantley, 1994; Gıslason, 2000), which compares favorably with estimates from this study.

Using a different approach, Armannsson (1991) estimated the total steam vent CO_2 flux of Icelandic geothermal systems to be ~3×10^9 mol a^{-1}, by extrapolating measured steam emissions rates in the Krafla geothermal region to other geothermal areas throughout Iceland. In addition, Arnórsson (1991) and later Arnórsson and Gıslason (1994) used heat flux estimates from Icelandic geothermal areas (Pálmason et al., 1985) to estimate steam emissions – assuming that convective flow of steam is the dominant heat transport mode in these areas. As with the previous approach, steam estimates were then combined with measured CO_2 steam contents to estimate a total CO_2 flux (2–5×10^{10} mol a^{-1}) for Iceland.

These various CO_2 flux estimates for Iceland – calculated using different methodologies – are summarized in Table 4 – and also compared to other plume-related and subaerial volcanic regions worldwide. We note that CO_2 output estimates from this study overlap with previous estimates for Iceland (Arnórsson, 1991; Gıslason, 1992; Arnórsson and Gıslason, 1994; Agustsdottir and Brantley, 1994; Gıslason, 2000) as well as estimates from other volcanically-active regions. For example, the CO_2 emissions from Iceland are bracketed by individual Italian volcanic

CO_2 output estimates which span from ~0.1 × 10^{10} mol a^{-1} at Solfatara, Italy (Chiodini et al., 1998) to ~100 × 10^{10} mol a^{-1} at Mt. Etna, Sicily (Allard et al., 1991; Brantley and Koepenick, 1995), the largest individual volcanic CO_2 emitter on Earth. Furthermore, the CO_2 flux from all of Iceland is comparable to previous estimates of ~6–7 × 10^{10} mol a^{-1} for the entire Central American Arc (Hilton, 2002; Shaw et al., 2003). CO_2 output estimates from this study also overlap with estimates made for other hotspot sources such as Réunion, Society Island, Pitcairn and Hawaii, which yield CO_2 fluxes between ~0.1 and 3.0 × 10^{10} mol a^{-1} (Greenland et al., 1985; Gerlach and Graeber, 1985; Bureau et al., 1998; Aubaud et al., 2005, 2006). In contrast, continental hotspot regions (e.g., Yellowstone) typically emit more CO_2, with estimates by Werner and Brantley (2003) (23–50 × 10^{10} mol a^{-1}) representing 2–25 times the total estimated for Iceland. In the context of other well-characterized, volcanically-active regions on Earth, this study clearly shows that Icelandic volcanism acts to transfer significant amounts of CO_2 from the mantle to Earth's surface.

6. CONCLUDING REMARKS

We report here a comprehensive survey of CO_2 characteristics (concentrations – both absolute values and relative to ^3He) of geothermal fluids and sub-glacial basalts obtained from on-axis and older off-axis portions of the Iceland crust. The principal findings of the study can be summarized as follows:

(1) LT geothermal samples from off-axis regions of the Icelandic crust possess more fractionated (i.e., lower $\delta^{13}C$ and $CO_2/^3He$) values vs. HT axial rift zone samples, indicating that calcite precipitation is a dominant process and a sink for CO_2 in the older and colder portions of the Icelandic crust.

(2) HT fluid samples of the ERZ display the highest geothermal $CO_2/^3He$ values measured. At localities where both fluid and gas phases were collected, fluid samples displayed up to two orders of magnitude higher $CO_2/^3He$ values vs. gas phases, suggesting that ERZ fluid samples have been affected by hydrothermal phase separation processes and that phase separation may be a pervasive processes affecting fluids throughout Iceland.

(3) Using subglacial basalt data, we are able to calculate pre-eruptive CO_2 source estimates for individual rift segments of Iceland, which show a general increase from the WRZ (206 ± 24 ppm) to the ERZ (371 ± 45 ppm) and reach a maximum in the NRZ (550 ± 66 ppm). Notably, uncertainty estimates assume no assimilation in samples used to define the Δ value and that all samples are derived from a homogenous starting composition. When all data for Iceland are compiled, an average pre-eruptive CO_2 source concentration of 400–531 ppm is estimated, which is in excellent agreement with previous estimates for the DMM (367–858 ppm; Marty, 2012) and the adjacently located Reykjanes (396 ppm ± 48; de Leeuw, 2007) and Kolbeinsey (400 ± 100 ppm; Macpherson et al., 2005a) ridges.

(4) Pre-eruptive $\delta^{13}C$ (δ_p) is estimated to be −2.5 ± 1.1‰ for all of the neovolcanic zone basalt samples, which is in good agreement with the average geothermal value of −3.1 ± 1.9‰, suggesting that geothermal carbon isotopes closely resemble the primary mantle composition of Iceland. Notably, these values overlap with DMM $\delta^{13}C$ values as well as those previously reported from analogous plume-related magmatic systems in the Society Islands (Aubaud et al., 2005) and Hawaii (e.g., Loihi Seamount; Exley et al., 1986; Kilauea; Gerlach and Taylor, 1990; Hilton et al., 1997), suggesting little difference in $\delta^{13}C$ between plume-influenced and DMM mantle sources. Some ($n = 8$) basalt samples display evidence for crustal assimilation by a ^{13}C depleted (organic/sedimentary) component.

(5) Flux estimates of CO_2 from Iceland were made using three independent approaches. The first two approaches produce an estimate between 0.2 and 23 × 10^{10} mol a^{-1} for the whole of Iceland. Notably, the various approaches are dependent on assumptions related to magma production rates and partial melting. These estimates represent 0.1–10% of the estimated global ridge flux (2.2 × 10^{12} mol CO_2 a^{-1}). The third approach is used to approximate the CO_2 output from the Köldukvíslabotnar region (ERZ), producing a CO_2 flux of ~0.9–1.8 × 10^8 mol CO_2 a^{-1} – consistent with estimates from other geothermal/volcanic regions.

ACKNOWLEDGMENTS

This work was supported by NSF grants EAR-0439122 and EAR-0537618 to D.R.H. In addition, EAR-1144559 supported P.H.B. during the review and revision process. We thank Tobias Fischer, Kareen Prade and Olafur Patrick Olafsson for assistance in sample collection, and we acknowledge Bjorn Oddsson for collecting the geothermal samples from Kverkfjoll. Colin Macpherson and two anonymous reviewers are thanked for thoughtful and thorough reviews, as is Pete Burnard for editorial handling.

APPENDIX A. SUPPLEMENTARY DATA

Supplementary data associated with this article can be found, in the online version, at http://dx.doi.org/10.1016/j.gca.2014.02.038.

REFERENCES

Agustsdottir A. M. and Brantley S. L. (1994) Volatile fluxes integrated over four decades at Grímsvötn volcano, Iceland. *J. Geophys. Res.* **99**, 9505–9522.

Allard P., Carbonelle J., Dajlevic D., Le Bronec J., Morel P., Robe M. C., Maurenas J. M., Faivre-Pierret R., Martin D., Sabroux J. C. and Zettwoog P. (1991) Eruptive and diffuse emissions of CO_2 from Mount Etna. *Nature* **351**, 387–391.

Allard P., Burton M. R., Oskarsson N., Michel A., and Polacci M. (2010) Chemistry and fluxes of magmatic gases powering the explosive trachyandesitic phase of Eyjafjallajokull 2010 eruption: Constraints on degassing magma volumes and processes. In *AGU Fall Meeting Abstracts* (Vol. 1, p. 07).

Armannsson H. (1991) Geothermal energy and the environment. In: Geoscience Society of Iceland. *Conference on Geology and Environmental Matters. Program and Abstracts*, pp. 16–17 (in Icelandic).

Armannsson H., Gislason G. and Torfason H. (1986) Surface exploration of the Theistareykir high-temperature geothermal area, Iceland, with special reference to the application of geochemical methods. *Appl. Geochem.* **1**, 47–64.

Armannsson H., Fridriksson T. and Kristjansson B. R. (2005) CO_2 emissions from geothermal power plants and natural geothermal activity in Iceland. *Geothermics* **34**, 286–296.

Arnórsson, S. (1991) Estimate of natural CO_2 and H_2S flow from Icelandic high-temperature geothermal areas. *Conference on Geology and Environmental Matters. Program and Abstracts*, pp. 18–19.

Arnórsson S. (1995) Geothermal systems in Iceland: structure and conceptual models-II. Low temperature areas. *Geothermics* **24**, 603–629.

Arnórsson S. and Barnes I. (1983) The nature of carbon dioxide waters in Snaefellsnes, western Iceland. *Geothermics* **12**, 171–176.

Arnórsson S. and Gıslason S. R. (1994) CO_2 from magmatic sources in Iceland. *Mineral. Mag.* **58A**, 27–28.

Arnórsson S., Axelsson G. and Sæmundsson K. (2008) Geothermal systems in Iceland. *Jökull* **58**, 269–302.

Aubaud C., Pineau F., Hékinian R. and Javoy M. (2005) Degassing of CO_2 and H_2O in submarine lavas from the Society hotspot. *Earth Planet. Sci. Lett.* **235**(3), 511–527.

Aubaud C., Pineau F., Hékinian R. and Javoy M. (2006) Carbon and hydrogen isotope constraints on degassing of CO_2 and H_2O in submarine lavas from the Pitcairn hotspot (South Pacific). *Geophys. Res. Lett.* **33**(2).

Barry P. H., Hilton D. R., Fischer T. P., de Moor J. M., Mangasini F. and Ramirez C. (2013) Helium and carbon isotope systematics of cold "mazuku" CO_2 vents and hydrothermal gases and fluids from Rungwe Volcanic Province, southern Tanzania. *Chem. Geol.* **339**, 141–156.

Bianchi D., Sarmiento J. L., Gnanadesikan A., Key R. M., Schlosser P. and Newton R. (2010) Low helium flux from the mantle inferred from simulations of oceanic helium isotope data. *Earth Planet. Sci. Lett.* **297**, 379–386.

Bijwaard H. and Spakman W. (1999) Tomographic evidence for a narrow whole mantle plume below Iceland. *Earth Planet. Sci. Lett.* **166**, 121–126.

Bjarnason I. T. and Schmeling H. (2009) The lithosphere and asthenosphere of the Iceland hotspot from surface waves. *Geophys. J. Int.* **178**(1), 394–418.

Bjarnason I. T., Menke W., Flovenz O. G. and Caress D. (1993) Tomographic image of the Mid-Atlantic plate boundary in southwestern Iceland. *J. Geophys. Res.* **98**, 6607–6622.

Bjarnason I. T., Wolfe C. J. and Solomon S. C. (1996) Initial results from the ICEMELT experiment: body-wave delay times and shear-wave splitting across Iceland. *Geophys. Res. Lett.* **23**, 459–462.

Bjornsson A. (1985) Dynamics of crustal rifting in Iceland. *J. Geophys. Res.* **90**, 151–162.

Bodvarsson G. (1961) Physical characteristics of natural heat resources in Iceland. *Jokull* **11**, 29–38.

Bottinga Y. (1969) Calculated fractionation factors for carbon and hydrogen isotope exchange in the system calcite–CO_2–graphite–methane–hydrogen and water vapour. *Geochim. Cosmochim. Acta* **33**, 49–64.

Bottinga Y. and Javoy M. (1990) MORB degassing: bubble growth and ascent. *Chem. Geol.* **81**(4), 255–270.

Brantley S. L. and Koepenick K. W. (1995) Measured carbon dioxide emissions from Oldoinyo Lengai and the skewed distribution of passive volcanic fluxes. *Geology* **23**, 933–936.

Breddam K., Kurz M. D. and Storey M. (2000) Mapping out the conduit of the Iceland mantle plume with helium isotopes. *Earth Planet. Sci. Lett.* **176**, 45–55.

Bureau H., Pineau F., Métrich N., Semet M. P. and Javoy M. (1998) A melt and fluid inclusion study of the gas phase at Piton de la Fournaise volcano (Réunion Island). *Chemical geology* **147**(1), 115–130.

Burnard P. and Harrison D. (2005) Argon isotope constraints on modification of oxygen isotopes in Iceland Basalts by surficial processes. *Chem. Geol.* **216**, 143–156.

Cartigny P. (2005) Stable isotopes and the origin of diamond. *Elements* **1**(2), 79–84.

Cartigny P., Boyd S., Harris J. and Javoy M. (1997) Nitrogen isotopes in peridotitic diamonds from Fuxian, China: the mantle signature. *Terra Nova* **9**(4), 175–179.

Cartigny P., Harris J. W., Phillips D., Girard M. and Javoy M. (1998) Subduction-related diamonds? The evidence for a mantle-derived origin from coupled $\delta^{13}C$-$\delta^{15}N$ determinations. *Chem. Geol.* **147**(1–2), 147–159.

Cartigny P., De Corte K., Shatsky V. S., Ader M., De Paepe P., Sobolev N. V. and Javoy M. (2001) The origin and formation of metamorphic microdiamonds from the Kokchetav massif, Kazakhstan: a nitrogen and carbon isotopic study. *Chem. Geol.* **176**(1), 265–281.

Chiodini G., Cioni R., Guidi M., Raco B. and Marini L. (1998) Soil CO_2 flux measurements in volcanic and geothermal areas. *Appl. Geochem.* **13**, 543–552.

Condomines M., Grönvold K., Hooker P. J., Muehlenbachs K., O'Nions R. K., Oskarsson N. and Oxburgh E. R. (1983) Helium, oxygen and strontium isotopic relationships in Icelandic volcanics. *Earth Planet. Sci. Lett.* **66**, 125–136.

Craig H., Clarke W. B. and Beg M. A. (1975) Excess ^3He in deep water on the East Pacific Rise. *Earth Planet. Sci. Lett.* **26**, 125–132.

Crisp J. A. (1984) Rates of magma emplacement and volcanic output. *J. Volcanol. Geotherm. Res.* **20**, 177–212.

Darbyshire F. A., White R. S. and Priestley K. F. (2000) Structure of the crust and uppermost mantle of Iceland from a combined seismic and gravity study. *Earth Planet. Sci. Lett.* **181**, 409–428.

Dasgupta R. and Hirschmann M. M. (2010) The deep carbon cycle and melting in Earth's interior. *Earth Planet. Sci. Lett.* **298**, 1–13.

de Leeuw G. A. M. (2007) The noble gas and carbon systematics of divergent, convergent and strike-slip plate boundaries: examples from the Reykjanes Ridge, Central American Arc and North Anatolian Fault Zone. Ph. D. thesis, University of California, San Diego.

Deines P., Harris J. W. and Gurney J. J. (1987) Carbon isotopic composition, nitrogen content and inclusion composition of diamonds from the Roberts Victor kimberlite, South Africa: Evidence for ^{13}C depletion in the mantle. *Geochimica et Cosmochimica Acta* **51**(5), 1227–1243.

Delacour A., Fruh-Green G. L., Bernasconi S. M., Schaeffer P. and Kelley D. S. (2008) Carbon geochemistry of serpentinites in the Lost City Hydrothermal System (30 N, MAR). *Geochim. Cosmochim. Acta* **72**, 3681–3702.

Delaney J. R., Muenow D. W. and Graham D. G. (1978) Abundance and distribution of water, carbon and sulfur in the glassy rims of submarine pillow basalts. *Geochim. Cosmochim. Acta* **42**, 581–594.

Delgado H., Piedad-Sanchez N., Galvian L., Julio P., Alvarez J. M. and Cardenas L. (1998) CO_2 flux measurements at Popocatepetl volcano: II. Magnitude of emissions and significance. *EOS Trans. Am. Geophys. Union* **79**, 926–971.

Des Marais D. J. and Moore J. G. (1984) Carbon and its isotopes in mid-oceanic basaltic glasses. *Earth Planet. Sci. Lett.* **69**(1), 43–57.

Dixon J. E. and Clague D. A. (2001) Volatiles in basaltic glasses from Loihi Seamount, Hawaii: evidence for a relatively dry plume component. *J. Petrol.* **42**(3), 627–654.

Dixon J. E. and Stolper E. M. (1995) An experimental study of water and carbon dioxide solubilities in mid-ocean ridge basaltic liquids. Part II: Applications to degassing. *J. Petrol.* **36**(6), 1633–1646.

Dubacq B., Bickle M. J. and Evans K. A. (2013) An activity model for phase equilibria in the H_2O-CO_2-NaCl system. *Geochim. Cosmochim. Acta* **110**, 229–252.

Ellam R. M. and Stuart F. M. (2004) Coherent He-Nd-Sr isotope trends in high $^3He/^4He$ basalts: implications for a common reservoir, mantle heterogeneity and convection. *Earth Planet. Sci. Lett.* **224**, 511–523.

Ellis A. J. and Golding R. M. (1963) The solubility of carbon dioxide above 100 degrees C in water and in sodium chloride solutions. *Am. J. Sci.* **261**(1), 47–60.

Exley R. A., Mattey D. P., Clague D. A. and Pillinger C. P. (1986) Carbon isotope systematics of a mantle hotspot: a comparison of Loihi seamount and MORB glasses. *Earth Planet. Sci. Lett.* **78**, 189–199.

Farley K. A., Maier-Reimer E., Schlosser P. and Broecker W. S. (1995) Constraints on mantle ^3He fluxes and deep-sea circulation from an oceanic general circulation model. *J. Geophys.* **100**, 3829–3839.

Fine G. and Stolper E. (1986) Dissolved carbon dioxide in basaltic glasses: concentration and speciation. *Earth Planet. Sci. Lett.* **76**(3–4), 263–278.

Fischer T. P., Burnard P., Marty B., Hilton D. R., Füri E., Palhol F., Sharp Z. D. and Mangasini F. (2009) Upper-mantle volatile chemistry at Oldoinyo Lengai volcano and the origin of carbonatites. *Nature* **459**(7243), 77–80.

Fisk M. R., Storrie-Lombardi M. C., Douglas S., Popa R., McDonald G. and Di Meo-Savoie C. (2003) Evidence of biological activity in Hawaiian subsurface basalts. *Geochem. Geophys. Geosyst.* **4**, 12.

Flower M. F. J., Pritchard R. G., Brem G., Cann J. R., Delaney J., Emmermann R., Gibson I. L., Oakley P. J., Robinson P. T. and Schmincke H. U. (1982) Chemical stratigraphy, Iceland Research Drilling Project Reydarfjordur, eastern Iceland. *J. Geophys. Res.* **87**, 6489–6510.

Foulger G. R., Pritchard M. J., Julian B. R., Evans J. R., Allen R. M., Nolet G., Morgan W. J., Bergsson B. H., Erlendsson P., Jakobsdottir S., Ragnarsson S., Stefansson R. and Vogfjord K. (2000) The seismic anomaly beneath Iceland extends down to the mantle transition zone and no deeper. *Geophys. J. Int.* **142**, F1–F5.

Foulger G. R., Pritchard M. J., Julian B. R., Evans J. R., Allen R. M., Nolet G., Morgan W. J., Bergsson B. H., Erlendsson P., Jakobsdottir S., Ragnarsson S., Stefansson R. and Vogfjord K. (2001) Seismic tomography shows that upwelling beneath Iceland is confined to the upper mantle. *Geophys. J. Int.* **146**, 504–530.

Fridleifsson I. B. (1979) Geothermal activity in Iceland. *Jökull* **29**, 47–56.

Fridriksson T., Kristjansson B. R., Armannsson H., Margretardottir E., Olafsdottir S. and Chiodini G. (2006) CO_2 emissions and heat flow through soil, fumaroles, and steam heated mud pools at the Reykjanes geothermal area, SW Iceland. *Appl. Geochem.* **21**, 1551–1569.

Friedman I., O'Neil J. and Cebula G. (1982) Two new carbonate stable isotope standards. *Geostand. Newslett.* **6**(1), 11–12.

Füri E., Hilton D. R., Halldórsson S. A., Barry P. H., Hahm D., Fischer T. P. and Grönvold K. (2010) Apparent decoupling of the He and Ne isotope systematics of the Icelandic mantle: the role of He depletion, melt mixing, degassing fractionation and air interaction. *Geochim. Cosmochim. Acta* **74**, 3307–3332.

Furnes H., Muehlebachs K., Torsvik T., Thorseth I. H. and Tumyr O. (2001) Microbial fractionation of carbon isotopes in altered basaltic glass from the Atlantc Ocean, Lau Basin and Costa Rica Rift. *Chem. Geol.* **173**, 313–330.

Gerlach T. M. (1991) Etna's greenhouse pump. *Nature* **315**, 352–353.

Gerlach T. M. and Graeber E. J. (1985) Volatile budget of Kilauea volcano. *Nature* **313**, 273–277.

Gerlach T. M. and Taylor B. E. (1990) Carbon isotope constraints on degassing of carbon dioxide from Kilauea volcano. *Geochim. Cosmochim. Acta* **54**, 2051–2058.

Gıslason S. R. (2000), Carbon dioxide from Eyjafjallajökull and Chemical Composition of SpringWater and River Water in the Eyjafjallajökull – Myrdalsjökull region. Science Institute, University of Iceland, Report RH-06-2000, 40.

Gıslason S. R., Andresdottir A., Sveinbjornsdottir A. E., Oskarsson N., Thordarson Th., Torssander P., Novak M. and Zak K. (1992) Local effects of volcanoes on the hydrosphere: example from Hekla, southern Iceland. In *Water-Rock Interaction* (eds. Y. K. Kharaka and A. S. Maest). Balkema, Rotterdam, pp. 477–481.

Greenland L. P., Rose W. I. and Stokes J. B. (1985) An estimate of gas emissions and magmatic gas content from Kilauea volcano. *Geochim. Cosmochim. Acta* **49**, 125.

Gysi A. P. and Stefánsson A. (2012) CO_2-water–basalt interaction. Low temperature experiments and implications for CO_2 sequestration into basalts. *Geochim. Cosmochim. Acta* **81**, 129–152.

Hahm D., Hilton D. R., Castillo P. R., Hawkins J. W., Hanan B. B. and Hauri E. H. (2012) An overview of the volatile systematics of the Lau Basin – resolving the effects of source variation, magmatic degassing and crustal contamination. *Geochim. Cosmochim. Acta* **85**, 88–113.

Hardarson B. S., Fitton J. G., Ellam R. M. and Pringle M. S. (1997) Rift relocation—a geochemical and geochronological investigation of a palaeo-rift in NW Iceland. *Earth Planet. Sci. Lett.* **153**, 181–195.

Hart S. R., Schilling J. G. and Powell J. L. (1973) Basalts from Iceland and along the Reykjanes Ridge: Sr isotope geochemistry. *Nat. Phys. Sci.* **246**(155), 104–107.

Hauri E. (2002) SIMS analysis of volatiles in silicate glasses, 2: isotopes and abundances in Hawaiian melt inclusions. *Chem. Geol.* **183**(1), 115–141.

Helmberger D., Wen L. and Ding X. (1998) Seismic evidence that the source of the Iceland hotspot lies at the core–mantle boundary. *Nature* **396**, 251–258.

Heng L. (2004) Preliminary environmental impact assessment for the Hágöngur high-temperature area, central Iceland. *The United Nations University: Geothermal Training Programme*, **10**.

Hilton D. R., Fischer T. P. and Marty B. (2002) Noble gases and volatile recycling at subduction zones. In *Noble Gases in Cosmochemistry and Geochemistry*, vol. 47 (eds. D. Porcelli, C. J. Ballentine and R. Wieler). Mineralogical Society of America, pp. 319–370.

Hilton D. R., Gronvold K., O'Nions R. K. and Oxburgh E. R. (1990) Regional distribution of ^3He anomalies in the Icelandic crust. *Chem. Geol.* **88**(1–2), 53–67.

Hilton D. R., Hammerschmidt K., Loock G. and Friedrichsen H. (1993) Helium and argon isotope systematics of the central Lau

Basin and Valu Fa Ridge: evidence of crust/mantle interactions in a backarc basin. *Geochim. Cosmochim. Acta* **57**, 2819–2841.

Hilton D. R., Barling J. and Wheller G. E. (1995) Effect of shallow-level contamination on the helium isotope systematics of ocean-island lavas. *Nature* **373**(6512), 330–333.

Hilton D. R., McMurtry G. M. and Kreulen R. (1997) Evidence for extensive degassing of the Hawaiian Mantle Plume from helium-carbon relationships at Kilauea Volcano. *Geophys. Res. Lett.* **24**(23), 3065–3068.

Hilton D. R., McMurtry G. M. and Goff F. (1998a) Large variations in vent fluid $CO_2/^3He$ ratios signal rapid changes in magma chemistry at Loihi seamount, Hawaii. *Nature* **396**, 359–362.

Hilton D. R., Grönvold K., Sveinbjornsdottir A. E. and Hammerschmidt K. (1998b) Helium isotope evidence for off-axis degassing of the Icelandic hotspot. *Chem. Geol.* **149**(3–4), 173–187.

Hilton D. R., Grönvold K., Macpherson C. G. and Castillo P. R. (1999) Extreme $^3He/^4He$ ratios in northwest Iceland: constraining the common component in mantle plumes. *Earth Planet. Sci. Lett.* **173**(1), 53–60.

Hoefs J. (2010) *Stable Isotope Geochemistry: Jochen Hoefs*. Springer.

Höskuldsson A., Sparks R. S. J. and Carroll M. R. (2006) Constraints on the dynamics of subglacial basalt eruptions from geological and geochemical observations at Kverkfjöll, NE-Iceland. *Bull. Volcanol.* **68**, 689–701.

Jakobsson S. P. and Gudmundsson M. T. (2008) Subglacial and intraglacial volcanic formations in Iceland. *Jökull* **58**, 179–197.

Jakobsson S. P., Jonasson K. and Sigurdsson I. A. (2008) The three igneous rock series of Iceland. *Jökull* **58**, 117–138.

Jambon A., Weber H. W. and Braun O. (1986) Solubility of He, Ne, Ar, Kr and Xe in a basalt melt in the range 1250–1600 °C. Geochemical implications. *Geochim. Cosmochim. Acta* **50**(3), 401–408.

Javoy M. (1997) The major volatile elements of the Earth: their origin, behavior, and fate. *Geophys. Res. Lett.* **24**(2), 177–180.

Javoy M. and Pineau F. (1991) The volatiles record of a "popping" rock from the Mid-Atlantic Ridge at 14 N: chemical and isotopic composition of gas trapped in the vesicles. *Earth Planet. Sci. Lett.* **107**(3), 598–611.

Javoy M., Pineau F. and Iiyama I. (1978) Experimental determination of the isotopic fractionation between gaseous CO_2 and carbon dissolved in tholeiitic magma; a preliminary study. *Contrib. Mineral. Petrol.* **67**, 35–39.

Jendrzejewski N., Trull T. W., Pineau F. and Javoy M. (1997) Carbon solubility in mid-ocean ridge basaltic melt at low pressures (250–1950 bar). *Chem. Geol.* **138**, 81–92.

Jóhannesson H. and K. Sæmundsson (1998) Geological map of Iceland. Bedrock geology, scale 1:500.000. Náttúrufræðistofnun Islands, Reykjavík (2nd edition).

Kerrick D. M. (2001) Present and past non-anthropogenic CO_2 degassing from the solid Earth. *Rev. Geophys.* **39**(4), 564–585.

Kristjansson B. R., Fridriksson Th. and Armannsson H. (2004) CO_2 emissions from Icelandic geothermal systems: geological constraints and preliminary results. *GFF* **126**(1), 153–154.

Kulongoski J. T. and Hilton D. R. (2002) A quadrupole-based mass spectrometric system for the determination of noble gas abundances in fluids. *Geochem. Geophys. Geosyst.* **3**(6), 1–10.

Kurz M. D., Meyer P. S. and Sigurdsson H. (1985) Helium isotopic systematics within the neovolcanic zones of Iceland. *Earth Planet. Sci. Lett.* **74**(4), 291–305.

Lang S. Q., Butterfield D. A., Lilley M. D., Johnson H. P. and Hedges J. I. (2006) Dissolved organic carbon in ridge-axis and ridge-flank hydrothermal systems. *Geochim. Cosmochim. Acta* **70**, 3830–3842.

Le Cloarec M. F. and Marty B. (1991) Volatile fluxes from volcanoes. *Terra Nova* **3**, 17–27.

Licciardi J. M., Kurz M. D. and Curtice J. M. (2007) Glacial and volcanic history of Icelandic table mountains from cosmogenic ^3He exposure ages. *Quat. Sci. Rev.* **26**(11), 1529–1546.

Lux G. (1987) The behavior of noble gases in silicate liquids: Solution, diffusion, bubbles and surface effects, with applications to natural samples. *Geochimica et Cosmochimica Acta* **51**(6), 1549–1560.

Macpherson C. G. and Mattey D. P. (1994) Carbon isotope variations of CO_2 in Lau Basin basalts and ferrobasalts. *Earth Planet. Sci. Lett.* **121**(3–4), 263–276.

Macpherson C. G., Hilton D. R., Sinton J. M., Poreda R. J. and Craig H. (1998) High $^3He/^4He$ ratios in the Manus backarc basin: implications for mantle mixing and the origin of plumes in the western Pacific Ocean. *Geology* **26**, 1007–1010.

Macpherson C. G., Hilton D. R., Newman S. and Mattey D. P. (1999) CO_2, $^{13}C/^{12}C$ and H_2O variability in natural basaltic glasses: A study comparing stepped heating and FTIR spectroscopic techniques. *Geochim. Cosmochim. Acta* **63**(11–12), 1805–1813.

Macpherson C. G., Hilton D. R., Mertz D. F. and Dunai T. J. (2005a) Sources, degassing, and contamination of CO_2, H_2O, He, Ne, and Ar in basaltic glasses from Kolbeinsey Ridge, North Atlantic. *Geochim. Cosmochim. Acta* **69**(24), 5729–5746.

Macpherson C. G., Hilton D. R., Day J. M. D., Lowry D. and Grönvold K. (2005b) High-$^3He/^4He$, depleted mantle and low-$\delta^{18}O$, recycled oceanic lithosphere in the source of central Iceland magmatism. *Earth Planet. Sci. Lett.* **233**, 411–427.

Macpherson C. G., Hilton D. R. and Hammerschmidt K. (2010) No slab-derived CO_2 in Mariana Trough back-arc basalts: implications for carbon subduction and for temporary storage of CO_2 beneath slow spreading ridges. *Geochim. Cosmochim. Acta* **11**, 11.

Marty B. (1995) Nitrogen content of the mantle inferred from N_2–Ar correlation in oceanic basalts. *Nature* **377**, 326–329.

Marty B. (2012) The origins and concentrations of water, carbon, nitrogen and noble gases on Earth. *Earth Planet. Sci. Lett.* **313**, 55–66.

Marty B. and Jambon A. (1987) $C/^3He$ in volatile fluxes from the solid Earth: implications for carbon geodynamics. *Earth Planet. Sci. Lett.* **83**, 16–26.

Marty B. and Tolstikhin I. N. (1998) CO_2 fluxes from mid-ocean ridges, arc and plumes. *Chem. Geol.* **145**, 233–248.

Marty B. and Zimmermann L. (1999) Volatiles (He, C, N, Ar) in mid-ocean ridge basalts: assesment of shallow-level fractionation and characterization of source composition. *Geochim. Cosmochim. Acta* **63**(21), 3619–3633.

Mattey D. P. (1991) Carbon dioxide solubility and carbon isotope fractionation in basaltic melt. *Geochim. Cosmochim. Acta* **55**(11), 3467–3473.

Mattey D. P., Carr R. H., Wright I. P. and Pillinger C. T. (1984) Carbon isotopes in submarine basalts. *Earth Planet. Sci. Lett.* **70**(2), 196–206.

Mattey D. P., Exley R. A. and Pillinger C. T. (1989) Isotopic composition of CO_2 and dissolved carbon in basalt glass. *Geochim. Cosmochim. Acta* **53**, 2377–2386.

McDougall I., Kristjansson L. and Saemundsson K. (1984) Magnetostratigraphy and geochronology of northwest Iceland. *J. Geophys. Res.* **89**, 7029–7060.

Metrich N., Sigurdsson H., Meyer P. S. and Devine J. D. (1991) The 1783 Lakagigar eruption in Iceland: geochemistry, CO_2 and sulfur degassing. *Contrib. Mineral. Petrol.* **107**(4), 435–447.

Momme P., Oskarsson N. and Keays R. R. (2003) Platinum-group elements in the Icelandic rift system: melting processes and mantle sources beneath Iceland. *Chem. Geol.* **196**, 209–234.

Moore J. G., Batchelder J. N. and Cunningham C. G. (1977) CO_2 filled vesicles in mid ocean basalt. *J. Volcanol. Geotherm. Res.* **2**, 309–327.

Morgan W. J. (1971) Convection plumes in the lower mantle. *Nature* **230**, 42–43.

Morner N. A. and Etiope G. (2002) Carbon degassing from the lithosphere. *Global Planet. Change* **33**, 185–203.

Muhlenbachs K., Anderson, Jr., A. T. and Sigvaldason G. E. (1974) Low ^{18}O basalts from Iceland. *Geochim. Cosmochim. Acta* **38**, 577–588.

Mysen B. O., Arculus R. J. and Eggler D. H. (1975) Solubility of carbon dioxide in melts of andesite, tholeiite, and olivine nephelinite composition to 30 kbar pressure. *Contrib. Mineral. Petrol.* **53**, 227–239.

O'Nions R. K. and Oxburgh E. R. (1988) Helium, volatile fluxes and the development of the continental crust. *Earth Planet. Sci. Lett.* **90**, 331–347.

Oskarsson N., Sigvaldason G. E. and Steinthorsson S. (1982) A dynamic model of rift zone petrogenesis and the regional petrology of Iceland. *J. Petrol.* **23**, 28–74.

Pálmason G., Johnsen G.V., Torfason H., Sæmundsson K, Ragnars K, Haraldsson G.I. and Halldórsson, G.K. (1985) *Assessment of Geothermal Energy in Iceland.* Orkustofnun OS-85076/JHD-10, 134 pp. (in Icelandic).

Palot M., Cartigny P., Harris J. W., Kaminsky F. V. and Stachel T. (2012) Evidence for deep mantle convection and primordial heterogeneity from nitrogen and carbon stable isotopes in diamond. *Earth and Planet. Sci. Lett.* **357**, 179–193.

Pan V., Holloway J. R. and Hervig R. L. (1991) The pressure and temperature dependence of carbon dioxide solubility in tholeiitic basalt melts. *Geochimica et Cosmochimica Acta* **56**, 1875–1883.

Peate D., Breddam W., Baker K., Kurz J. A., Barker M. D., Prestvik A. K., Grassineau N. and Skovgaard A. C. (2010) Compositional characteristics and spatial distribution of enriched Icelandic mantle components. *J. Petrol.* **51**(7), 1447–1475.

Pineau F., Javoy M. and Bottinga Y. (1976) $^{13}C/^{12}C$ ratios of rocks and inclusions in popping-rocks of the mid-atlantic ridge and their bearing on the problem of isotopic composition of deep-seated carbon. *Earth Planet. Sci. Lett.* **29**, 413–421.

Porcelli D. and Wasserburg G. J. (1995) Mass transfer of helium, neon, argon, and xenon through a steady-state upper mantle. *Geochim. Cosmochim. Acta* **59**, 4921-493.

Poreda R. J., Craig H., Arnórsson S. and Welhan J. A. (1992) Helium isotopes in Icelandic geothermal systems: I. ^{3}He, gas chemistry, and ^{13}C relations. *Geochim. Cosmochim. Acta* **56**(12), 4221–4228.

Ray M. C., Hilton D. R., Muñoz J., Fischer T. P. and Shaw A. M. (2009) The effects of volatile recycling, degassing and crustal contamination on the helium and carbon geochemistry of hydrothermal fluids from the Southern Volcanic Zone of Chile. *Chem. Geol.* **266**, 38–49.

Ritsema J., van Heijst H. J. and Woodhouse J. H. (1999) Complex shear wave velocity structure imaged beneath Africa and Iceland. *Science* **286**, 1925–1928.

Saal A. L., Hauri E. H., Langmuir C. H. and Perfit M. R. (2002) Vapour undersaturation in primitive mid-ocean-ridge basalt and the volatile content of Earth's upper mantle. *Nature* **419**, 451–455.

Sano Y. and Marty B. (1995) Origin of carbon in fumarolic gas from island arcs. *Chem. Geol.* **119**(1), 265–274.

Sano Y. and Williams S. N. (1996) Fluxes of mantle and subducted carbon along convergent plate boundaries. *Geophys. Res. Lett.* **23**(20), 2749–2752.

Sano Y., Urabe A., Wakita H., Chiba H. and Sakai H. (1985) Chemical and isotopic compositions of gases in geothermal fluids in Iceland. *Geochem. J.* **19**, 135–148.

Schilling J. G. (1973) Iceland mantle plume: geochemical study of Reykjanes Ridge. *Nature* **242**, 565–571.

Schilling J. G., Unni C. K. and Bender M. L. (1978) Origin of chlorine and bromine in the oceans. *Nature* **273**, 631–636.

Shaw A. M., Hilton D. R., Fischer T. P., Walker J. A. and Alvarado G. (2003) Contrasting He–C relationships in Nicaragua and Costa Rica: insights into C cycling through subduction zones. *Earth Planet. Sci. Lett.* **214**, 499–513.

Shaw A. M., Hilton D. R., Macpherson C. G. and Sinton J. M. (2004) The CO_2–He–Ar–H_2O systematics of the Manus back–arc basin: resolving source composition from degassing and contamination effects. *Geochim. Cosmochim. Acta* **68**(8), 1837–1855.

Shilobreeva S., Martinez I., Busigny V., Agrinier P. and Laverne C. (2011) Insights into C and H storage in the altered oceanic crust: results from ODP/IODP Hole 1256D. *Geochim. Cosmochim. Acta* **75**(9), 2237–2255.

Slater L., Jull M., McKenzie D. and Grönvold K. (1998) Deglaciation effects on mantle melting under Iceland: results from the northern zone. *Earth Planet. Sci. Lett.* **164**, 151–164.

Stolper E. and Holloway J. R. (1988) Experimental determination of the solubility of carbon dioxide in molten basalt at low pressure. *Earth Planet. Sci. Lett.* **87**, 397–408.

Stracke A. and Bourdon B. (2009) The importance of melt extraction for tracing mantle heterogeneity. *Geochim. Cosmochim. Acta* **73**, 218–238.

Sun S. S., Tatsumoto M. and Schilling J. G. (1975) Mantle plume mixing along the Reykjanes Ridge axis: lead isotopic evidence. *Science* **190**(4210), 143–147.

Thirlwall M. F., Gee M. A. M., Taylor R. N. and Murton B. J. (2004) Mantle components in Iceland and adjacent ridges investigated using double-spike Pb isotope ratios. *Geochim. Cosmochim. Acta* **68**(2), 361–386.

Thirlwall M. F., Gee M. A. M., Lowry D., Mattey D. P., Murton B. J. and Taylor R. N. (2006) Low $\delta^{18}O$ in the Icelandic mantle and its origins: evidence from Reykjanes Ridge and Icelandic lavas. *Geochim. Cosmochim. Acta* **70**(4), 993–1019.

Thorseth I. H., Furnes H. and Heldal M. (1992) The importance of microbiological activity in the alteration of natural basaltic glass. *Geochim. Cosmochim. Acta* **56**, 845–850.

Tryggvason K., Husebye E. S. and Stefansson R. (1983) Seismic image of the hypothesized Icelandic hot spot. *Tectonophysics* **100**(1–3), 97–118.

Tuffen H., Owen J. and Denton J. (2010) Magma degassing during subglacial eruptions and its use to reconstruct palaeo-ice thicknesses. *Earth Sci. Rev.* **99**(1–2), 1–18.

Van Soest M. C., Hilton D. R. and Kreulen R. (1998) Tracing crustal and slab contributions to arc magmatism in the Lesser Antilles island arc using helium and carbon relationships in geothermal fluids. *Geochim. Cosmochim. Acta* **62**(19), 3323–3335.

Varekamp J. C., Kreulen R., Poorter R. P. E. and Van Bergen M. J. (1992) Carbon sources in arc volcanism, with implications for the carbon cycle. *Terra Nova* **4**, 363–373.

Wardell L. J. and Kyle P. R. (1998) Volcanic carbon dioxide emission rates: White Island, New Zealand and Mt. Erebus, Antarctica (abstract). *EOS Trans. AGU* **79**(45), 927 (Fall Meeting Suppl.).

Weiss R. F. (1971) Solubility of helium and neon in water and seawater. *J. Chem. Eng. Data* **16**(2), 235–241.

Werner C. and Brantley S. (2003) CO_2 emissions from the Yellowstone volcanic system. *Geochem. Geophys. Geosyst.* **4**, 27.

White R. S. (1993) Melt production rates in mantle plumes. *Philos. Trans. R. Soc. London* **A342**, 137–153.

White R. S., Bown J. W. and Smallwood J. R. (1995) The temperature of the Iceland plume and origin of outward-propagating V-shaped ridges. *J. Geol. Soc. London* **152**, 1039–1045.

Williams S. N., Schaefer S. J., Calvache M. L. and Lopez D. (1992) Global carbon dioxide emission to the atmosphere by volcanoes. *Geochim. Cosmochim. Acta* **56**, 1765–1770.

Wolfe C., Bjarnason I., VanDecar J. and Soloman S. (1997) Seismic structure of the Iceland mantle plume. *Nature* **385**, 245–247.

Zhao D. P. (2004) Global tomographic images of mantle plumes and subducting slabs: insight into deep Earth dynamics. *Phys. Earth Planet. Inter.* **146**(1–2), 3–34.

Associate editor: Pete Burnard